Air quality and health impacts of Data Center electricity demand in the United States

Yuang Chen[1,2], Shen Wang[3,4], Juan Ramon L Senga[3,5], Andrew Scott White[1,6], Anthony YH Wong[1], Lyssa M Freese[7], Michelle L Bell[8], Noelle E Selin[1,2,9]

[1] Center for Sustainability Science and Strategy, Massachusetts Institute of Technology, Cambridge, MA, United States of America
[2] Institute for Data, Systems and Society, Massachusetts Institute of Technology, Cambridge, MA, United States of America
[3] Center for Energy and Environmental Policy Research, Massachusetts Institute of Technology, Cambridge, MA, United States of America
[4] MIT Energy Initiative, Massachusetts Institute of Technology, Cambridge, MA, United States of America
[5] MIT Climate Policy Center, Massachusetts Institute of Technology, Cambridge, MA, United States of America
[6] Laboratory for Aviation and the Environment, Department of Aeronautics and Astronautics, Massachusetts Institute of Technology, Cambridge, MA, United States of America
[7] Department of Earth System Science, University of California, Irvine, Irvine, CA, United States of America
[8] School of the Environment, Yale University, New Haven, Connecticut, United States of America
[9] Department of Earth, Atmospheric, and Planetary Sciences, Massachusetts Institute of Technology, Cambridge, MA, United States of America

E-mail: yuang007@mit.edu

This manuscript has been submitted for review in *Environmental Research Letters*. If accepted, the final version of this manuscript will be available via the 'Peer-reviewed Publication DOI' link on the right-hand side of the EarthArxiv web page for the paper.

Abstract.

The rapid expansion of artificial intelligence is associated with a substantial growth in electricity demand from data centers in the US, yet the resulting air quality and public health impacts remain poorly quantified. Data centers represent large, near-continuous demands that fundamentally alter power system dispatch and emissions. To quantify the ambient air pollution and associated premature mortality impacts of grid-supplied data center electricity demand in 2023, we couple the United States Electricity Generation Optimization (US-EGO) model with the GEOS-Chem chemical transport model. Our results show that electricity generation attributable to data center demand is largely supplied by fossil fuel units across multiple regions, resulting in additional annual mean $PM_{2.5}$ concentrations of 0.02–0.08 μg m^{-3} (local peak concentrations up to $\sim$0.2 μg m^{-3}), and regionally varying ozone responses characterized by wintertime

depletion and summertime enhancement. These impacts are most pronounced in the Midwest United States, where marginal emissions from coal-fired units and ammonia-rich atmospheric conditions enhance secondary particulate formation. We estimate that this grid-supplied demand is responsible for 513 (95% CI: 469–557) annual premature mortalities from $PM_{2.5}$ and an additional 137 (95% CI: 90–183) annually from maximum daily 8-hour average ozone (MDA8-O_3) in the continental US. State- and county-level analyses reveal a systematic mismatch between where data center load is hosted and where associated mortality burdens occur. The spatial distribution of these adverse air quality impacts is driven by regional generation mixes, inter-regional electricity flows, and atmospheric transport, rather than local proximity to data centers. These results show that sustained computing demand adds air quality health burdens through coupled energy and environmental systems, highlighting the necessity of incorporating air quality into data center siting and macro-energy system planning.

Keywords: Data Center, Air Quality, Health, Electricity systems

1. Introduction

The rapid expansion of artificial intelligence (AI) has driven substantial growth in electricity demand from data centers in the United States [1–4]. Data centers are already among the most energy-intensive building types, with electricity consumption dominated by computing equipment and cooling systems [5, 6]. Recent estimates indicate that US data centers consumed approximately 150–200 TWh of electricity in 2023, representing roughly 4% of national electricity demand [7], with continued growth expected as major technology firms accelerate investment in hyperscale data centers, which are large-scale facilities supporting cloud computing and AI workloads [8–10]. This rapid increase has heightened concerns about the environmental implications of data center electricity consumption [11–13].

Prior research shows that the environmental footprint of data centers is driven by rapidly growing electricity demand and supporting infrastructure. Early estimates placed US data center emissions at roughly 0.5% of national greenhouse gas emissions [12], while more recent analyses indicate that electricity use reached ≈4.4% of US demand in 2023 [7]. Facility-level studies show that this demand is spatially concentrated and often served by fossil-intensive generation, yielding carbon intensities that can exceed national averages [11]. Cooling and water requirements introduce additional constraints: evaporative cooling can substantially increase freshwater consumption relative to air-cooled designs, creating tradeoffs between electricity efficiency and water use [6]. Water demand can also be temporally and spatially uneven, with peak withdrawals that strain local supply systems [14]. Together, these studies characterize aggregate impacts of data center growth but neglect the resulting changes in emissions, atmospheric chemistry, and population exposure that determine air quality and health outcomes.

Electricity generation induced by data center demand emits nitrogen oxides (NO_x), sulfur dioxide (SO_2), and primary particulate matter. These emissions contribute to fine particulate matter ($PM_{2.5}$) through direct emissions and secondary aerosol formation, while NO_x also influences ground-level ozone (O_3) through atmospheric photochemistry. Both pollutants are associated with premature mortality and other adverse health outcomes [15, 16]. Air quality damages from power-sector emissions are substantial, contributing to public health burdens worldwide [17–20]. Statistical analyses show that emissions and damages associated with marginal electricity demand vary widely across regions and hours, implying that the impacts of additional electricity consumption depend strongly on when and where demand occurs [21, 22]. Dispatch-based frameworks couple power system and air quality models to trace how demand changes propagate through generation, emissions, and exposure, showing that shifts in electricity demand can produce large and often non-local health impacts through regional electricity supply and atmospheric transport [23–26]. Together, these studies provide a mechanistic basis for linking electricity demand to pollution exposure.

Emerging work has begun to assess the air quality implications of electricity-intensive digital computing. Studies of cryptocurrency mining show that large, geographically concentrated computing loads can generate substantial air pollution damages through their interaction with power systems. Using grid-average emission factors, Goodkind et al. estimate that Bitcoin mining generated approximately $0.49 in combined health and climate damages for every $1 of market value produced in 2018 [27]. Guidi et al. further link increases in Bitcoin mining activity to higher fossil generation, identifying coal- and gas-fired units as key marginal suppliers in affected regions [28]. Extending beyond cryptocurrency, Han et al. estimate that emissions from data center electricity use and backup generation caused approximately 400 premature deaths in the US in 2023, rising to 1,300 annually by 2028–2030 [29]. Muller similarly estimates that data center electricity consumption in 2025 generated approximately $25 billion in annual external damages in the United States, including $4.6 billion from local air pollution, using facility-level loads and grid-average emissions rates [30]. These studies demonstrate that computing-driven electricity demand can impose substantial air quality burdens, but primarily rely on grid-average, statistical, or life-cycle approaches that do not resolve how data center loads alter dispatch, emissions timing, and downwind exposure.

Here we quantify the air quality and mortality impacts of grid-supplied electricity demand from US data centers in 2023. We couple a unit-level electricity dispatch model [26] with a chemical transport model [31, 32] to estimate changes in $PM_{2.5}$ and O_3 attributable to data center electricity use and translate these changes into premature mortality using established epidemiological relationships. This framework captures how data center electricity demand propagates through power system operations, emissions, and atmospheric transport, providing a policy-relevant baseline for assessing the environmental implications of continued data center expansion.

2. Materials and Methods

2.1. Data center electricity demand data

We estimate US data center electricity demand in 2023 using state-level consumption shares reported by the Electric Power Research Institute (EPRI) [33], which quantify data center electricity use as a fraction of total state electricity demand. These shares are mapped to US Environmental Protection Agency Integrated Planning Model (IPM) regions [34], which are based on balancing authority boundaries rather than state borders. Detailed mappings and resulting regional shares are provided in the Supporting Information (SI).

We assume hourly data center load within each IPM region is uniform throughout the year, consistent with the near-continuous operation of many large-scale data centers [35, 36]. All data center electricity demand is assumed to be supplied by the utility grid; on-site backup generation is not represented.

2.2. Electricity dispatch modeling

We simulate electricity system responses to data center electricity demand using the United States Electricity Generation Optimization (US-EGO) model, a plant-level, hourly least-cost dispatch framework that simulates electricity generation and interregional transmission across the contiguous United States [26, 37]. US-EGO has been used to attribute emissions from changes in electricity demand and generate inputs for downstream air quality modeling [38]. The model generates hourly CO_2, NO_x, and SO_2 emissions at the level of individual electricity generating units (EGUs).

For this study, we update the baseline US-EGO framework from its original 2016 electricity system representation to reflect 2023 grid conditions and generator operating constraints relevant to sustained data center loads. Model inputs are updated to reflect the current generator fleet, regional electricity demand, transmission constraints, and renewable energy availability using publicly available data sources [34]. In contrast to earlier implementations that relied on economic dispatch, we incorporate a chronological dispatch formulation with operating constraints to better represent the limited flexibility of large thermal units. Specifically, coal and natural gas combined-cycle (NGCC) generators are represented using minimum stable output levels and intertemporal ramp-rate limits [39, 40]. This linearized approximation to unit commitment preserves computational tractability while better capturing short-run generator responses to persistent changes in net load from near-continuous data center demand [41, 42]. The model also includes intertemporal constraints for energy storage and hydro reservoir operations [43, 44], linking resource availability across hours and allowing dispatch to reflect system flexibility over time. Detailed model formulation, parameterization, and data sources are provided in the SI.

We attribute electricity generation and emissions to data center demand using a with-without counterfactual approach, solving US-EGO with observed 2023 demand and

again with data center load removed. Differences in generator dispatch and emissions represent the marginal response to data center electricity consumption.

2.3. Air quality modeling

We quantify air quality impacts using the GEOS-Chem High Performance (GCHP) model (version 14.4.0), a global three-dimensional model that simulates atmospheric transport, chemistry, and deposition [31, 32, 45]. We conduct full-chemistry simulations, including detailed coupled gas-phase and aerosol chemistry, using the GCHP stretched-grid capability [46]. The model is run on a global cubed-sphere grid with native C48 resolution, corresponding to approximately 200 km grid spacing on an unstretched grid. A stretch factor of 3.0 centered at 40°N, 91°W increases effective resolution over the contiguous United States to approximately 50 km while retaining a global domain. The model employs 72 vertical layers extending from the surface to 0.01 Pa (∼80 km altitude). Meteorological fields are taken from the MERRA-2 reanalysis [47], and simulations include a six-month spin-up period.

Emissions are processed using the Harmonized Emissions Component (HEMCO) [48]. Anthropogenic emissions within the contiguous United States, excluding SO_2 and NO_x from EGUs, are based on a modified 2016 National Emissions Inventory (NEI) adjusted from NEI 2011 [49]. EGU emissions are replaced with those simulated by US-EGO. Global anthropogenic emissions outside the United States are taken from Community Emissions Data System (CEDS) version 2, and all other emission sources follow the standard GCHP 14.4.0 configuration (https://gchp.readthedocs.io/en/14.4.0/user-guide/configuration-files.html).

We evaluate baseline GCHP performance by comparing simulated annual mean secondary $PM_{2.5}$ and MDA8-O_3 concentrations against observations from the US Environmental Protection Agency Air Quality System (AQS). The model reproduces broad spatial patterns across the United States, with moderate correlation and biases ($PM_{2.5}$: $R = 0.41$, bias $= +1.15$ μg m^{-3}; O_3: $R = 0.65$, bias $= +6.3$ ppb) consistent with prior GEOS-Chem evaluations, which attribute similar model-observation differences to uncertainties in emissions, atmospheric chemistry, and meteorology [50–52]. As our analysis focuses on differences between counterfactual scenarios, systematic biases in baseline concentrations are expected to largely cancel and therefore do not materially affect estimated air quality and health impacts. Additional evaluation, including spatial maps, monitor-level comparisons, and residual diagnostics, is provided in the SI.

In addition to GCHP, we use the Intervention Model for Air Pollution (InMAP) Source-Receptor Matrix (ISRM), a reduced-form air quality model, to provide a structural comparison of $PM_{2.5}$ responses. The ISRM is derived from InMAP and represents atmospheric transport and chemistry using linearized source-receptor relationships that estimate concentration changes resulting from emissions in each source region [53]. Owing to its computational efficiency, this framework has been widely used to evaluate air quality impacts of alternative policy and emissions scenarios [54, 55],

though it does not fully capture the nonlinear atmospheric chemistry represented in chemical transport models such as GCHP. Given emissions of primary $PM_{2.5}$, SO_x, NO_x, NH_3, and volatile organic compounds (VOCs), the ISRM estimates annual-average total $PM_{2.5}$ concentrations [56]. It provides spatially resolved concentration responses on a variable-resolution grid over the contiguous United States. Comparisons between GCHP- and ISRM-based estimates are discussed in Section 4.

2.4. Health impact assessment

We estimate health impacts associated with data center electricity demand by translating modeled changes in ground-level $PM_{2.5}$ and O_3 concentrations into premature mortality. Mortality impacts are calculated using concentration-response functions (CRFs) that relate changes in long-term pollutant exposure to relative mortality risk. For $PM_{2.5}$, we apply the Global Exposure Mortality Model (GEMM) for non-communicable diseases and lower respiratory infections [57]. For O_3, we use a log-linear CRF for all-cause and respiratory mortality based on changes in long-term exposure to maximum daily 8-hour average ozone (MDA8-O_3) concentration [58]. Additional assumptions and computational details are provided in the SI. Reported uncertainty ranges are derived from CRF uncertainty and do not include uncertainties associated with emissions or air quality modeling.

To characterize the distribution of attributable health impacts across demographic and geographic groups, we compiled census tract-level demographic and socioeconomic data from the 2018–2022 American Community Survey (ACS) 5-year estimates. Variables included population counts by race and ethnicity, median household income, and poverty indicators. Urbanicity was characterized using United States Department of Agriculture Rural-Urban Commuting Area (RUCA) classifications, aggregated into urban and non-urban categories, where non-urban includes suburban and rural tracts. Attributable mortality estimates were spatially allocated to census tracts based on gridded population distributions and linked with tract-level demographic attributes to evaluate disparities in exposure and health burden across population groups.

To characterize spatial patterns relative to data center infrastructure, we compiled facility-level data center information from the Data Center Atlas [59]. We also obtained county-level data center capacity estimates derived from aggregated Baxtel infrastructure data through the National Laboratory of the Rockies mapping API associated with the DOE Speed to Power initiative [60], downloaded in December 2025. County-level analyses evaluated relationships between attributable mortality and distance to the nearest large-scale data center facility, as well as differences across electricity market regions and among counties hosting, neighboring, or farther from data center infrastructure.

3. Results

3.1. Spatial distribution of data center electricity demand

In 2023, data center electricity demand is highly concentrated in a small number of US states, both in loads and as a share of total state electricity consumption (Figure 1a). Virginia and Texas account for the largest absolute data center loads (33.9 and 21.8 TWh, respectively), reflecting the clustering of hyperscale and colocation facilities in Northern Virginia and major metropolitan regions of Texas. Additional states with notable demand include California (9.3 TWh), Illinois (7.5 TWh), and Oregon (6.4 TWh). The share of state electricity demand attributable to data centers varies widely. In Virginia, data centers account for 25.6% of total state electricity consumption, far exceeding the national average of 3.8% and all other states. Several states with more moderate absolute loads, including Iowa and Nebraska, also exhibit high relative shares (11.4% and 11.7%, respectively), driven by lower baseline electricity demand. This heterogeneity implies that data center growth affects regional electricity systems through both large load additions and substantial shifts in local demand composition.

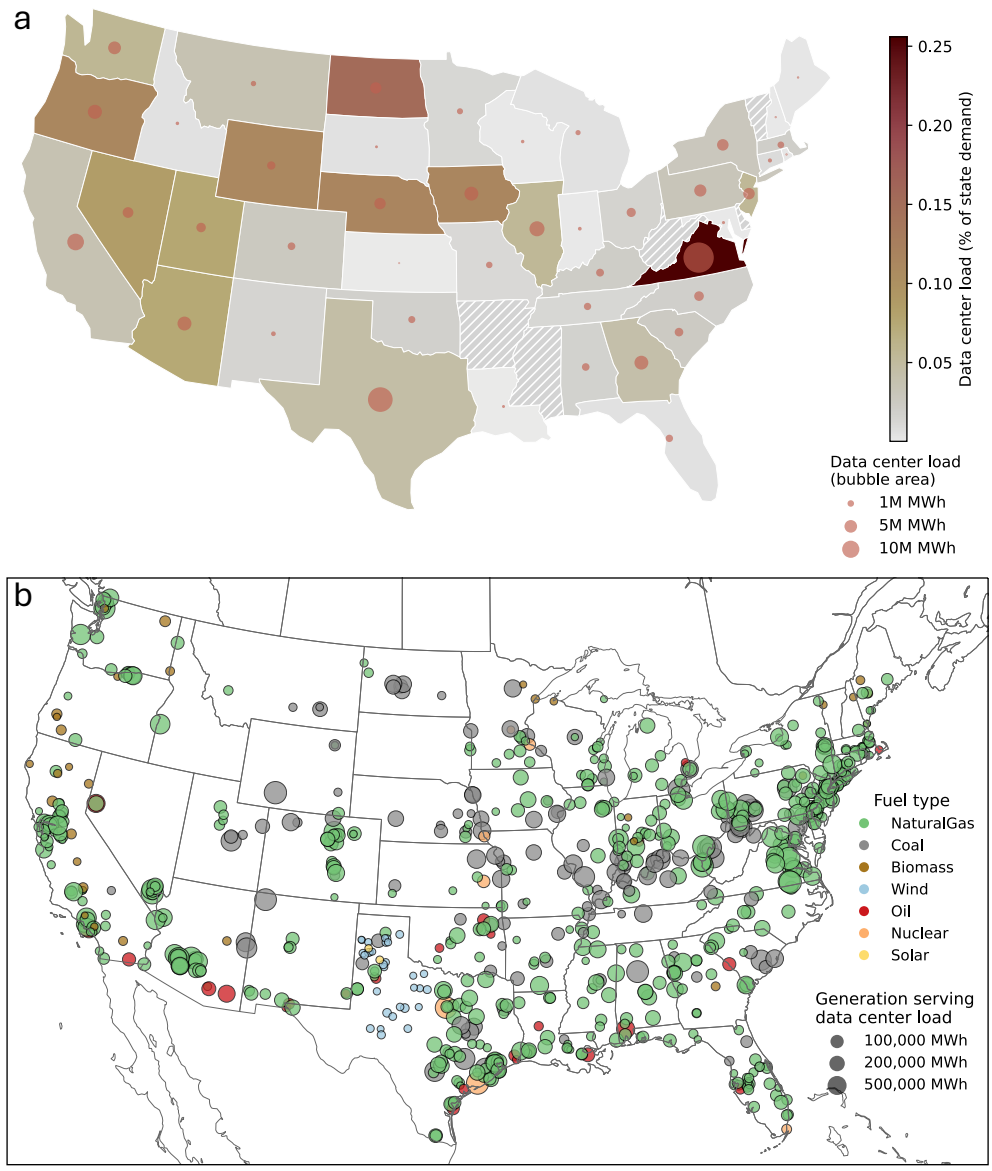

Figure 1: Spatial distribution of data center electricity demand and associated electricity generation in 2023. (a) State-level data center electricity demand across the United States. Bubble area indicates total annual data center electricity consumption, and color shading indicates data center load as a share of total state electricity demand. (b) Electricity-generating units (EGUs) supplying data center load under modeled dispatch conditions. Circle area is proportional to annual attributable generation serving data center electricity demand, and colors indicate fuel type.

3.2. Generation mix and emissions attributable to data center demand

Grid-supplied electricity demand from US data centers in 2023 drives 171.0 TWh of generation, equivalent to 3.81% of total US grid output. The resulting emissions represent larger shares of power-sector totals: 103.5 Tg CO_2 (6.69%), 61.4 kt NO_x (7.32%), and 39.1 kt SO_2 (5.63%), reflecting the emissions-intensive nature of marginal

electricity supply. Natural gas and coal dominate attributable generation and emissions across most regions (Figure 1b). A large share of attributable SO_2 and NO_x emissions originates from coal-fired units in the Midwest, indicating that data center demand is frequently met by emissions-intensive generation.

Peaking units account for a disproportionate share of NO_x emissions relative to their generation contribution. Peaking units are defined as generators with annual capacity factors below 15% and nameplate capacities exceeding 10 MW, following [61]. These units supply approximately 4% of attributable generation but account for 7% of attributable NO_x emissions.

3.3. Air quality impacts attributable to data center electricity demand

Annual-mean $PM_{2.5}$ attributable to data center electricity demand is highest in the central United States and Midwest, with smaller but widespread impacts across the eastern United States (Figure 2a). Annual-mean $\Delta PM_{2.5}$ is typically 0.02–0.08 μg m^{-3} across much of the central and eastern US, with localized maxima approaching $\sim$0.2 μg m^{-3}. These perturbations are small relative to baseline $PM_{2.5}$ concentrations (5–12 μg m^{-3} across the United States; Figure S2), but are comparable to concentration changes associated with policy-relevant emission shifts reported in prior studies and contribute to meaningful population exposure [21, 26]. As described in Methods, the spatial pattern of $\Delta PM_{2.5}$ is robust to GCHP baseline bias because it is only weakly explained by baseline residuals (Figure S3). Broadly elevated $PM_{2.5}$ across the Midwest and Ohio Valley reflects enhanced secondary inorganic aerosol formation under ammonia-rich conditions, with nitrate accounting for the dominant share of the response (Figure S4). The high $PM_{2.5}$ response in Nebraska and Iowa is also driven by marginal generation from individual coal-fired units dispatched in response to data center electricity demand that exhibit high NO_x and SO_2 emission rates (Figure S5). Several of these aging units were expected to retire but remain operational through 2025 [62]. Regions with substantial data center load, including the Electric Reliability Council of Texas (ERCOT) and PJM Interconnection (see Figure S7 for electricity market locations), also experience elevated $PM_{2.5}$ concentrations. However, these impacts are distributed across interconnected generation and transmission networks rather than confined to local demand centers.

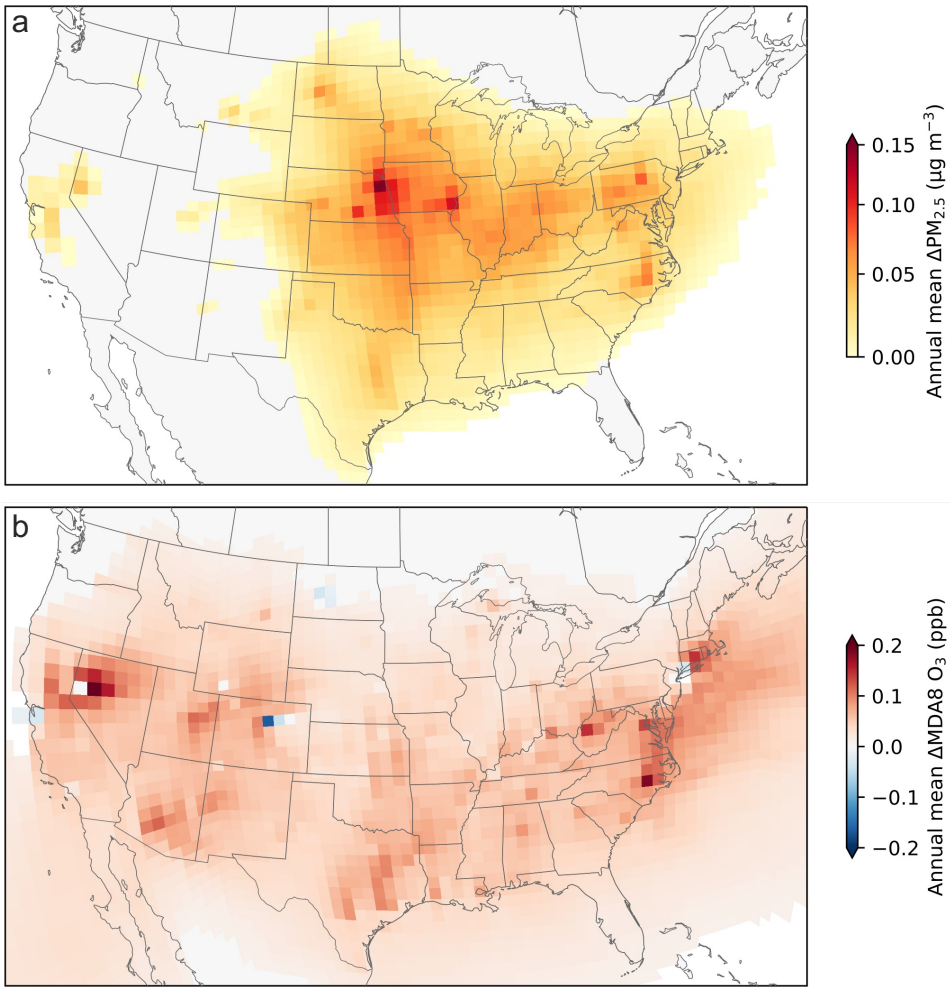

Figure 2: Annual mean air quality responses attributable to US data center electricity demand in 2023. (a) Change in surface $PM_{2.5}$ concentration. (b) Change in surface MDA8-O_3 concentration.

The ozone response to data center-attributable electricity generation exhibits strong seasonal patterns driven by the chemical regime governing ozone formation. In winter, incremental NO_x emissions from marginal generators generally reduce MDA8-O_3 (Figure S6), particularly in the Mid-Atlantic and Colorado Front Range, where high background NO_x concentrations and low biogenic volatile organic compound (BVOC) emissions favor ozone titration. In summer, when BVOC emissions are higher and ozone production is predominantly NO_x-limited across much of the United States, the same NO_x perturbations lead to widespread increases in MDA8-O_3, often displaced downwind of emitting regions by regional transport (Figure S6). Summer ozone production dominates the annual mean signal, while wintertime reductions provide only partial local compensation, resulting in a net positive annual mean ozone response across most populated regions (Figure 2b).

3.4. Premature mortality burden and distributional patterns

Data center electricity demand is estimated to result in 513 (95% CI: 469–557) premature deaths annually from $PM_{2.5}$ and 137 (95% CI: 90–183) from MDA8-O_3, totaling 650 (95% CI: 559–740) attributable premature deaths per year. Mortality burdens are concentrated in densely populated regions of the Northeast, Mid-Atlantic, and Midwest, extending well beyond regions of high data center concentration due to atmospheric transport and electricity transmission.

State-level analysis reveals a systematic mismatch between where data center load is hosted and where mortality burden occurs (Figure 3). Virginia and Texas host the largest absolute data center loads but exhibit only moderate attributable mortality rates per capita. In Virginia, additional demand is met by generation distributed across the broader PJM Interconnection, dispersing associated impacts beyond state boundaries. Texas, by contrast, relies primarily on in-state generation within ERCOT, resulting in higher total attributable mortality despite a lower per-capita mortality rate. States with large data center loads relative to the size of their electricity systems (Figure 1a), particularly Nebraska and Iowa, experience some of the highest attributable mortality rates, reaching 6.5 deaths per million population in Nebraska, consistent with the air quality patterns described in Section 3.3. More strikingly, states with minimal data center presence, including Kansas, South Dakota, Missouri, and Arkansas, also exhibit elevated mortality rates (upper left quadrant of Figure 3). Table S1 further shows that the contribution of data center-attributable mortality to total EGU-attributable mortality is relatively similar across states despite large differences in local data center load. This pattern indicates that mortality impacts are not confined to states hosting data center infrastructure but are distributed across interconnected electricity and atmospheric transport pathways.

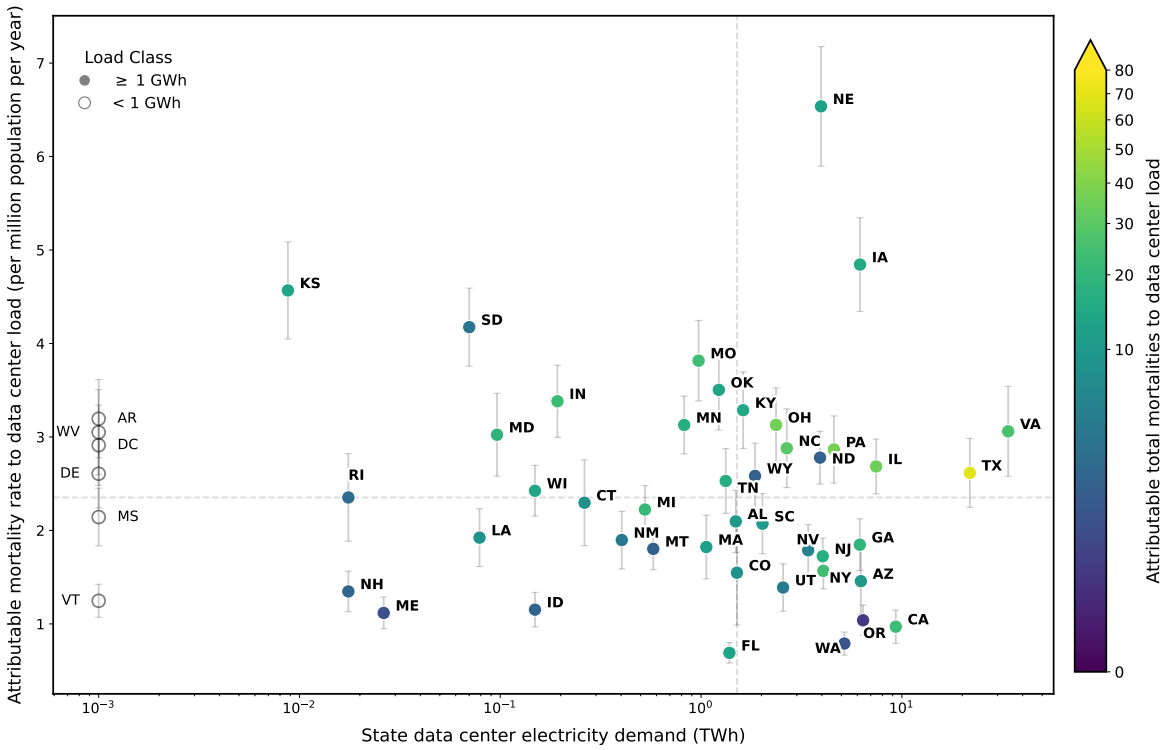

Figure 3: State-level data center electricity demand versus attributable premature mortality rates (deaths per million population per year). Colors indicate total state-level mortalities attributable to data center electricity demand. Dashed lines denote the median state-level data center electricity demand and attributable mortality rate, dividing states into four quadrants for comparison. Open circles indicate states with annual data center electricity demand below 1 GWh; these states are plotted at 10^{-3} TWh for visualization purposes.

To assess whether mortality burdens are concentrated near data center facilities, we classify counties within each major electricity market as hosting, neighboring, or farther from hyperscale facilities and compare attributable mortality rates across categories (Figure S7). Within most markets, including PJM, Southeast, and ERCOT, mortality rate distributions overlap substantially across all three county classes, with no consistent elevation in hosting counties. Modest differences appear in the Western Electricity Coordinating Council (WECC) and Southwest Power Pool (SPP), but within-category variance is large. A regression of county-level mortality rates against distance to the nearest large-scale data center yields a statistically significant but negligibly small gradient of -0.192 deaths per 100,000 per 100 km, with heterogeneous slopes across individual markets (Figures S8 and S9). Together, these results indicate that mortality impacts from data center electricity demand are widely distributed across the population instead of being concentrated near hosting facilities. This reflects the structure of grid-supplied electricity impacts, where effects arise primarily from EGU emissions distributed across balancing authorities rather than local facility sources. Localized

impacts from on-site generation, such as backup diesel use, are not represented here and may lead to underestimation of near-facility exposures.

Based on differences in exposure patterns, attributable mortality rates also exhibit systematic demographic and urbanicity-related differences. Nationally, non-urban populations experience higher attributable mortality rates, at 0.27 deaths per 100,000 people (95% CI: 0.24-0.31), compared to 0.21 deaths per 100,000 (95% CI: 0.19-0.25) for urban populations (Figure 4a). White and American Indian/Alaska Native (AIAN) populations also experience relatively high mortality rates (both approximately 0.24 deaths per 100,000), whereas Hispanic and Asian populations experience lower rates (0.18 and 0.19 deaths per 100,000, respectively). This pattern differs from findings for the broader electricity sector, where Black populations often experience the highest exposure burdens [54]. However, within-state disparities are considerably smaller. Relative to state-average attributable mortality rates, most racial and ethnic groups exhibit differences centered near zero across states (Figure 4b). The largest AIAN outliers, including Nevada and Colorado, reflect spatial overlap between subgroup populations and within-state mortality hotspots rather than uniformly elevated mortality burdens (Figure S10). In contrast, elevated mortality rates among non-urban populations persist across many states (Figure 4c), indicating a more spatially consistent urbanicity effect. Together, these patterns suggest that demographic disparities are driven primarily by the geography of emissions-intensive electricity generation and regional population distributions rather than proximity to data center facilities. Income-based differences are comparatively small, ranging from 0.21 to 0.24 deaths per 100,000 across quintiles. These disparities are likely underestimated, as our method accounts for differences in exposure but not differential vulnerability. Earlier research suggests that some subpopulations, including racial/ethnic minorities and lower socioeconomic groups, may experience greater health risks from equivalent levels of air pollution exposure [63].

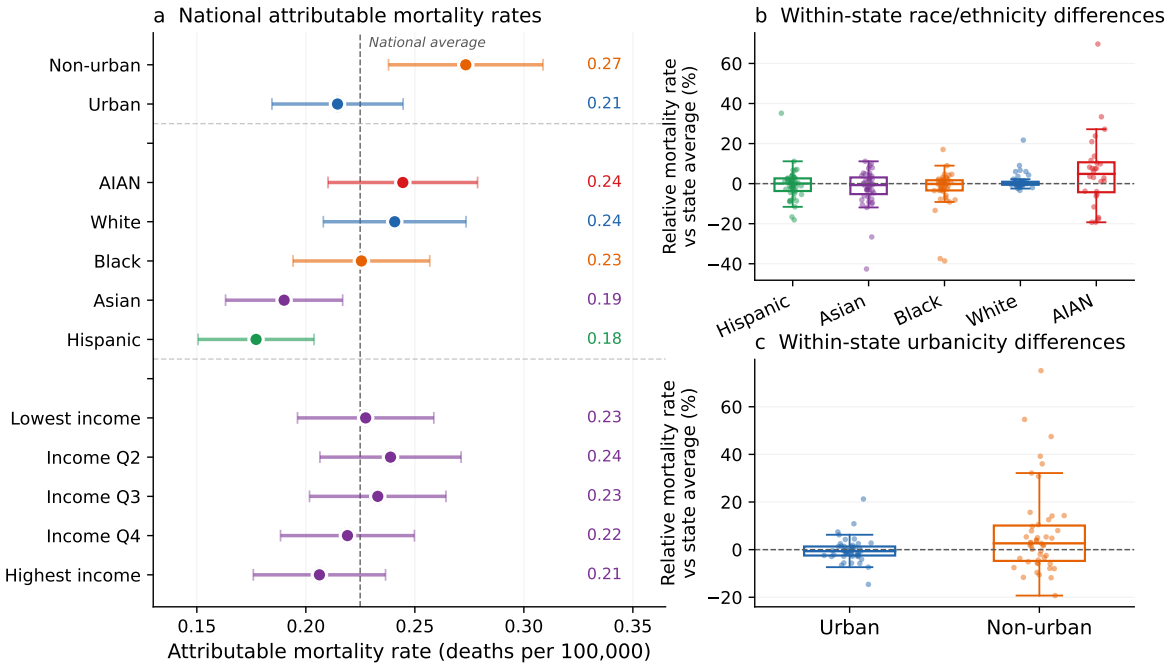

Figure 4: Distributional patterns in premature mortality attributable to US data center electricity demand based on differences in exposure. (a) Population-weighted mortality rates across urbanicity, racial/ethnic, and income groups. (b) Within-state relative mortality rate differences across racial/ethnic groups relative to state-wide average mortality rates. (c) Within-state relative mortality rate differences between urban and non-urban populations relative to state-wide average mortality rates. Points represent individual states and boxplots show the interquartile range and median across states. Urbanicity categories are based on Rural-Urban Commuting Area (RUCA) tract classifications. Income quintiles are defined using tract-level median household income from the American Community Survey.

4. Discussion

This study quantifies the air quality and health impacts associated with US data center electricity demand by linking plant-level hourly dispatch modeling with three-dimensional atmospheric chemistry simulations. We estimate resulting changes in $PM_{2.5}$, O_3, and premature mortality across the contiguous United States. By integrating electricity system operations with full-chemistry air quality modeling, we identify regions that experience a disproportionate share of impacts and show that digital infrastructure growth has measurable public health consequences. Data center electricity demand accounts for approximately 3.8% of total US electricity generation but is associated with 650 (95% CI: 559–740) premature deaths annually, compared to 12,247 (95% CI: 10,599–13,893) deaths from total power-sector emissions, representing 5.3% of electricity-related air pollution mortality.

Our attribution is based on a with-without framework that quantifies how the

electricity system responds to data center demand, rather than allocating emissions using regional-average or generation-weighted mixes. While average-based approaches assign data centers the emissions intensity of existing generation [11, 30], they do not estimate the incremental emissions caused by additional electricity consumption. Because our goal is to quantify air quality and health impacts attributable to data center electricity demand, we focus on the resulting changes in generation and emissions that directly determine exposure and health outcomes.

Our estimates reflect grid-mediated emissions associated with continuous data center electricity demand and do not include on-site backup generator operation. Backup units are typically diesel-fired and operate occasionally for testing or reliability events. Although annual runtime is limited, their emission intensities are high; prior estimates suggest that backup generator use contributes on the order of $\sim$30 deaths annually compared to around 400 from grid-supplied electricity under typical operating assumptions [29]. In addition, while current behind-the-meter generation remains small ($\leq$3 GW) relative to grid-supplied load [64], planned expansion of on-site generation capacity could increase the importance of local emissions in future deployments [65]. Our findings therefore likely underestimate near-facility air quality and health impacts surrounding large data centers. Furthermore, the approximately 50 km horizontal resolution of the air quality simulations is designed to capture regional-scale impacts and may not fully resolve localized exposure gradients near individual power plants or data centers. Previous work has identified environmental justice concerns related to the siting of electricity infrastructure and peaking power plants [61]. Future studies using finer-resolution modeling could better quantify these local-scale impacts and assess whether they amplify the demographic disparities identified here.

We compare results from the full-chemistry GCHP simulation with those from the reduced-form ISRM framework (Figure S11). GCHP resolves nonlinear secondary inorganic aerosol chemistry and attributes the Midwest $PM_{2.5}$ response primarily to nitrate formation under ammonia-rich conditions. In contrast, ISRM relies on source-receptor relationships calibrated to 2005–2010 background emissions and chemistry, whereas US NO_x and SO_2 emissions have declined substantially over the past decade, altering present-day chemical regimes (Figure S12). These differences in chemistry and background conditions produce spatial discrepancies, particularly in regions where marginal emissions affect nitrate formation. This sensitivity is especially relevant for emerging loads such as data centers, which may shift emissions in regions without historically large pollution signals.

These findings have direct implications for data center siting, operation, and regulatory oversight. Integrating air quality considerations into siting, permitting, and grid planning could help reduce unintended health impacts, particularly in communities already exposed to elevated pollution levels. More broadly, our results show that air quality impacts extend well beyond data center locations, contrasting with the more localized water-use and noise impacts highlighted in previous studies [14, 66]. As data center electricity demand continues to grow, incorporating plant-level emissions

responses into infrastructure planning will be important for aligning digital expansion with public health and environmental goals.

Data availability statement

The data that support the findings of this study are openly available at the following URL/DOI: 10.5281/zenodo.20681107.

Acknowledgments

Y.C. was supported by the MIT Energy Initiative Society of Energy Scholars and the MIT Martin Family Society of Fellows for Sustainability. J.R.L.S. and S.W. were supported by funding from the Future Energy Systems Center of the MIT Energy Initiative (MITei). A.S.W. was supported by the National Science Foundation Graduate Research Fellowship under Grant No. 1745302. Any opinions, findings, and conclusions or recommendations expressed in this material are those of the authors and do not necessarily reflect the views of the National Science Foundation. The authors thank Christopher Knittel for insightful discussions and acknowledge helpful feedback from participants of the Doctoral Student Participatory Workshop on Climate and Energy Decision Making at Carnegie Mellon University. The MERRA-2 data used in this research were provided by the Global Modeling and Assimilation Office (GMAO) at NASA Goddard Space Flight Center. Computations were performed on the Svante cluster at the Massachusetts Green High Performance Computing Center, supported by the MIT Center for Sustainability Science and Strategy.

References

[1] Gang He. Renewable integration and ai demand reshape power grids. *Nat. Rev. Clean Technol.*, 2(1):13–14, 2026.

[2] International Energy Agency. Energy and ai. https://www.iea.org/reports/energy-and-ai/energy-demand-from-ai, 2025. Accessed: YYYY-MM-DD.

[3] Tyler H. Norris, Tim Profeta, Dalia Patino-Echeverri, and Adam Cowie-Haskell. Rethinking load growth: Assessing the potential for integration of large flexible loads in us power systems. Technical report, Nicholas Institute for Energy, Environment and Sustainability, Duke University, 2025. Accessed April 7, 2025.

[4] Caishan Guo, Fengji Luo, Zexiang Cai, and Zhao Yang Dong. Integrated energy systems of data centers and smart grids: State-of-the-art and future opportunities. *Appl. Energy*, 301:117474, 2021.

[5] Eric Masanet, Arman Shehabi, Nuoa Lei, Sarah Smith, and Jonathan Koomey. Recalibrating global data center energy-use estimates. *Science*, 367(6481):984–986, 2020. Accessed April 7, 2025.

[6] Zhen Li and Satish G. Kandlikar. Current status and future trends in data-center cooling technologies. *Heat Transfer Engineering*, 36(6):523–538, 2015. Publisher: Taylor & Francis. Accessed April 9, 2025.

[7] Arman Shehabi, Sarah Smith, Alex Hubbard, Alex Newkirk, Nuoa Lei, Md Abu Bakkar Siddik, Billie Holecek, Jonathan Koomey, Eric Masanet, and Dale Sartor. 2024 united states data center energy usage report. Technical report, Lawrence Berkeley National Laboratory, December 2024. Accessed April 9, 2025.

[8] OpenAI. Announcing the stargate project. https://openai.com/index/announcing-the-stargate-project/, January 2025. Accessed: 2026-01-31.

[9] Reuters. Google plans $40 billion texas data center investment amid ai boom. https://www.reuters.com/business/google-invest-40-billion-new-data-centers-texas-bloomberg-news-reports-2025-11-14/, November 2025. Accessed: 2026-01-31.

[10] Carlo Brancucci, Dylan Cutler, and Jesse Jenkins. Flexible data centers: A faster, more affordable path to power. Technical report, Camus and Encoord and Princeton ZERO Lab, December 2025. White paper.

[11] Gianluca Guidi, Francesca Dominici, Jonathan Gilmour, Kevin Butler, Eric Bell, Scott Delaney, and Falco J. Bargagli-Stoffi. Environmental burden of united states data centers in the artificial intelligence era, 2024. arXiv preprint.

[12] Md Abu Bakar Siddik, Arman Shehabi, and Landon Marston. The environmental footprint of data centers in the united states. *Environmental Research Letters*, 16(6):064017, 2021. Publisher: IOP Publishing. Accessed April 7, 2025.

[13] Christopher R Knittel, Juan Ramon L Senga, and Shen Wang. Flexible data centers and the grid: Lower costs, higher emissions? Technical report, National Bureau of Economic Research, 2025. NBER Working Paper.

[14] Yuelin Han, Pengfei Li, Adam Wierman, and Shaolei Ren. Small bottle, big pipe: Quantifying and addressing the impact of data centers on public water systems. *arXiv preprint arXiv:2603.02705*, 2026.

[15] D. T. Shindell. The social cost of atmospheric release. *Clim. Change*, 130(2):313–326, 2015.

[16] L. Henneman, C. Choirat, I. Dedoussi, F. Dominici, J. Roberts, and C. Zigler. Mortality risk from united states coal electricity generation. *Science*, 382(6673):941–946, 2023.

[17] J. Heo, P. J. Adams, and H. O. Gao. Public health costs of primary $PM_{2.5}$ and inorganic $PM_{2.5}$ precursor emissions in the united states. *Environ. Sci. Technol.*, 50(11):6061–6070, 2016.

[18] J. Lelieveld, K. Klingmüller, A. Pozzer, R. T. Burnett, A. Haines, and V. Ramanathan. Effects of fossil fuel and total anthropogenic emission removal on public health and climate. *Proc. Natl. Acad. Sci. U.S.A.*, 116(15):7192–7197, 2019.

[19] Paulina Jaramillo and Nicholas Z Muller. Air pollution emissions and damages from energy production in the us: 2002–2011. *Energy Policy*, 90:202–211, 2016.

[20] Ruili Wu, Fei Liu, Dan Tong, Yixuan Zheng, Yu Lei, Chaopeng Hong, Meng Li, Jun Liu, Bo Zheng, Yu Bo, et al. Air quality and health benefits of china's emission control policies on coal-fired power plants during 2005–2020. *Environmental Research Letters*, 14(9):094016, 2019.

[21] Minghao Qiu, Corwin M. Zigler, and Noelle E. Selin. Impacts of wind power on air quality, premature mortality, and exposure disparities in the united states. *Sci. Adv.*, 8:eabn8762, 2022.

[22] Duncan S. Callaway, Meredith Fowlie, and Gavin McCormick. Location, location, location: The variable value of renewable energy and demand-side efficiency resources. *J. Assoc. Environ. Resour. Econ.*, 5:39–75, 2018.

[23] K. Siler-Evans, I. L. Azevedo, and M. G. Morgan. Marginal emissions factors for the us electricity system. *Environ. Sci. Technol.*, 46(9):4742–4748, 2012.

[24] D. W. Abel, T. Holloway, J. Martínez-Santos, M. Harkey, M. Tao, C. Kubes, and S. Hayes. Air quality-related health benefits of energy efficiency in the united states. *Environ. Sci. Technol.*, 53(7):3987–3998, 2019.

[25] A. Bin Thaneya and A. Horvath. Exploring regional fine particulate matter ($PM_{2.5}$) exposure reduction pathways using an optimal power flow model: The case of the illinois power grid. *Environ. Sci. Technol.*, 57(21):7989–8001, 2023.

[26] L. M. Freese, G. P. Chossière, S. D. Eastham, A. Jenn, and N. E. Selin. Nuclear power generation phase-outs redistribute us air quality and climate-related mortality risk. *Nat. Energy*, 8(5):492–503, 2023.

[27] Andrew L. Goodkind, Benjamin A. Jones, and Robert P. Berrens. Cryptodamages:

Monetary value estimates of the air pollution and human health impacts of cryptocurrency mining. *Energy Res. Soc. Sci.*, 59:101281, 2020.

[28] Gianluca Guidi, Francesca Dominici, Nat Steinsultz, Gabriel Dance, Lucas Henneman, Henry Richardson, Edgar Castro, Falco J. Bargagli-Stoffi, and Scott Delaney. The environmental burden of the united states' bitcoin mining boom. *Nature Communications*, 16(1):2970, 2025. Publisher: Nature Publishing Group. Accessed April 7, 2025.

[29] Yuelin Han, Zhifeng Wu, Pengfei Li, Adam Wierman, and Shaolei Ren. The unpaid toll: Quantifying and addressing the public health impact of data centers. *arXiv preprint arXiv:2412.06288*, 2024.

[30] Nicholas Z. Muller. Measuring the impact of data centers in the united states economy: Monetary damage from air pollution and greenhouse gas emissions. NBER Working Paper 35100, National Bureau of Economic Research, Cambridge, MA, 2026.

[31] I. Bey, D. J. Jacob, R. M. Yantosca, J. A. Logan, B. D. Field, A. M. Fiore, Q. Li, H. Y. Liu, L. J. Mickley, and M. G. Schultz. Global modeling of tropospheric chemistry with assimilated meteorology: Model description and evaluation. *J. Geophys. Res. Atmos.*, 106(D19):23073–23095, 2001.

[32] S. D. Eastham, M. S. Long, C. A. Keller, E. Lundgren, R. M. Yantosca, J. Zhuang, C. Li, C. J. Lee, M. Yannetti, B. M. Auer, T. L. Clune, J. Kouatchou, W. M. Putman, M. A. Thompson, A. L. Trayanov, A. M. Molod, R. V. Martin, and D. J. Jacob. GEOS-Chem High Performance (gchp v11-02c): A next-generation implementation of the GEOS-Chem chemical transport model for massively parallel applications. *Geosci. Model Dev.*, 11(7):2941–2953, 2018.

[33] Electric Power Research Institute. Powering intelligence: Analyzing artificial intelligence and data center energy consumption. Technical report, Electric Power Research Institute (EPRI), 2024. Accessed April 9, 2025.

[34] US Environmental Protection Agency. Epa's power sector modeling platform v6 using ipm summer 2021 reference case. https://www.epa.gov/power-sector-modeling/epas-power-sector-modeling-platform-v6-using-ipm-summer-2021-reference-case, 2021. Accessed: March 31, 2025.

[35] Yihong Zhou, Angel Paredes, Chaimaa Essayeh, and Thomas Morstyn. AI-focused HPC data centers can provide more power grid flexibility and at lower cost, December 2024. Accessed April 29, 2025.

[36] Kaiyu Sun, Na Luo, Xuan Luo, and Tianzhen Hong. Prototype energy models for data centers. *Energy Build.*, 231:110603, 2021.

[37] A. Jenn. The future of electric vehicle emissions in the united states. Presented at the Transportation Research Board 97th Annual Meeting, Washington, DC, 2018. Paper No. 18-03325.

[38] Yuang Chen, Florian Allroggen, Sebastian D. Eastham, Evan M. Gibney, William C. Clark, and Noelle E. Selin. Air quality impacts of electricity purchase and air travel by organizations. *Environ. Res. Lett.*, 20:124056, 2025.

[39] Joshua A. Taylor. *Convex Optimization of Power Systems*. Cambridge University Press, 2015.

[40] Bernard Knueven, James Ostrowski, and Jean-Paul Watson. On mixed-integer programming formulations for the unit commitment problem. *INFORMS J. Comput.*, 32(4):857–876, 2020.

[41] Bowen Hua, Ross Baldick, and Jianhui Wang. Representing operational flexibility in generation expansion planning through convex relaxation of unit commitment. *IEEE Trans. Power Syst.*, 33(2):2272–2281, 2017.

[42] Kris Poncelet, Erik Delarue, and William D'haeseleer. Unit commitment constraints in long-term planning models: relevance, pitfalls, and the role of assumptions on flexibility. *Appl. Energy*, 258:113843, 2020.

[43] Brady Stoll, Juan Andrade, Stuart Cohen, Greg Brinkman, and Carlo Martinez-Anido Brancucci. Hydropower modeling challenges. Technical report, National Renewable Energy Laboratory, 2017.

[44] Ramteen Sioshansi, Paul Denholm, Juan Arteaga, Sarah Awara, Shubhrajit Bhattacharjee, Audun Botterud, Wesley Cole, Andres Cortés, Anderson De Queiroz, Joseph DeCarolis, et al. Energy-storage modeling: State-of-the-art and future research directions. *IEEE Trans. Power Syst.*, 37:860–875, 2021.

[45] R. V. Martin, S. D. Eastham, L. Bindle, E. W. Lundgren, T. L. Clune, C. A. Keller, W. Downs, D. Zhang, R. A. Lucchesi, M. P. Sulprizio, R. M. Yantosca, Y. Li, L. Estrada, W. M. Putman, B. M. Auer, A. L. Trayanov, S. Pawson, and D. J. Jacob. Improved advection, resolution, performance, and community access in the new generation (version 13) of the high-performance GEOS-Chem global atmospheric chemistry model (gchp). *Geosci. Model Dev.*, 15(23):8731–8748, 2022.

[46] L. Bindle, R. V. Martin, M. J. Cooper, E. W. Lundgren, S. D. Eastham, B. M. Auer, T. L. Clune, H. Weng, J. Lin, L. T. Murray, J. Meng, C. A. Keller, W. M. Putman, S. Pawson, and D. J. Jacob. Grid-stretching capability for the GEOS-Chem 13.0.0 atmospheric chemistry model. *Geosci. Model Dev.*, 14(10):5977–5997, 2021.

[47] R. Gelaro, W. McCarty, M. J. Suárez, R. Todling, A. Molod, L. Takacs, C. A. Randles, A. Darmenov, M. G. Bosilovich, R. Reichle, et al. The modern-era retrospective analysis for research and applications, version 2 (merra-2). *J. Clim.*, 30(14):5419–5454, 2017.

[48] C. A. Keller, M. S. Long, R. M. Yantosca, A. M. da Silva, S. Pawson, and D. J. Jacob. Hemco v1.0: A versatile, esmf-compliant component for calculating emissions in atmospheric models. *Geosci. Model Dev.*, 7(4):1409–1417, 2014.

[49] B. Henderson and L. Freese. Preparation of geos-chem emissions from cmaq, 2021.

[50] Yanshun Li, Randall V. Martin, Chi Li, Brian L. Boys, Aaron van Donkelaar, Jun Meng, and Jeffrey R. Pierce. Development and evaluation of processes affecting simulation of diel fine particulate matter variation in the geos-chem model. *Atmos. Chem. Phys.*, 23(19):12525–12543, 2023.

[51] JM Walker, S Philip, RV Martin, and JH Seinfeld. Simulation of nitrate, sulfate, and ammonium aerosols over the united states. *Atmos. Chem. Phys.*, 12(22):11213–11227, 2012.

[52] Katherine R. Travis and Daniel J. Jacob. Systematic bias in evaluating chemical transport models with maximum daily 8 h average (mda8) surface ozone for air quality applications: A case study with geos-chem v9.02. *Geosci. Model Dev.*, 12(8):3641–3648, 2019.

[53] Christopher W. Tessum, Jason D. Hill, and Julian D. Marshall. Inmap: A model for air pollution interventions. *PLoS One*, 12:e0176131, 2017.

[54] M. P. S. Thind, C. W. Tessum, I. L. Azevedo, and J. D. Marshall. Fine particulate air pollution from electricity generation in the us: Health impacts by race, income, and geography. *Environ. Sci. Technol.*, 53(23):14010–14019, 2019.

[55] Paul Picciano, Minghao Qiu, Sebastian D. Eastham, Mei Yuan, John Reilly, and Noelle E. Selin. Air quality related equity implications of u.s. decarbonization policy. *Nat. Commun.*, 14:5543, 2023.

[56] A. L. Goodkind, C. W. Tessum, J. S. Coggins, J. D. Hill, and J. D. Marshall. Fine-scale damage estimates of particulate matter air pollution reveal opportunities for location-specific mitigation of emissions. *Proc. Natl. Acad. Sci. U.S.A.*, 116(18):8775–8780, 2019.

[57] R. Burnett, H. Chen, M. Szyszkowicz, N. Fann, B. Hubbell, III Pope, C. A., J. S. Apte, M. Brauer, A. Cohen, S. Weichenthal, J. Coggins, Q. Di, B. Brunekreef, J. Frostad, S. S. Lim, H. Kan, K. D. Walker, G. D. Thurston, R. B. Hayes, C. C. Lim, M. C. Turner, M. Jerrett, D. Krewski, S. M. Gapstur, W. R. Diver, B. Ostro, D. Goldberg, D. L. Crouse, R. V. Martin, P. Peters, L. Pinault, M. Tjepkema, A. van Donkelaar, P. J. Villeneuve, A. B. Miller, P. Yin, M. Zhou, L. Wang, N. A. H. Janssen, M. Marra, R. W. Atkinson, H. Tsang, T. Q. Thach, J. B. Cannon, R. T. Allen, J. E. Hart, F. Laden, G. Cesaroni, F. Forastiere, G. Weinmayr, A. Jaensch, G. Nagel, H. Concin, and J. V. Spadaro. Global estimates of mortality associated with long-term exposure to outdoor fine particulate matter. *Proc. Natl. Acad. Sci. U.S.A.*, 115(38):9592–9597, 2018.

[58] M. C. Turner, M. Jerrett, III Pope, C. A., D. Krewski, S. M. Gapstur, W. R. Diver, B. S. Beckerman, J. D. Marshall, J. Su, D. L. Crouse, et al. Long-term ozone exposure and mortality in a large prospective study. *Am. J. Respir. Crit. Care Med.*, 193(10):1134–1142, 2016.

[59] K. Mongird, T. Thurber, C. Vernon, C. Burleyson, K. Z. Akdemir, and J. Rice. Im3 open source data center atlas (v2026.02.09), 2026.

[60] U.S. Department of Energy. Speed to power data viewer. https://web.archive.org/web/20251110062917/https://maps.nrel.gov/speed-to-power/, 2025. Archived by the Internet Archive Wayback Machine; accessed December 2025.

[61] U.S. Government Accountability Office. Electricity infrastructure: Information on disparities associated with energy infrastructure siting and federal efforts to address environmental justice concerns. Technical Report GAO-24-106145, U.S. Government Accountability Office, 2024. Accessed June 2026.

[62] Nebraska Public Media. Oppd again delays plan to stop burning coal at north omaha plant. *Nebraska Public Media*, 2026.

[63] Kevin P. Josey, Scott W. Delaney, Xiao Wu, Rachel C. Nethery, Priyanka DeSouza, Danielle Braun, and Francesca Dominici. Air pollution and mortality at the intersection of race and social class. *New England Journal of Medicine*, 388(15):1396–1404, 2023.

[64] Global Energy Monitor. Betting big on data centers: U.s. now leads world for new gas power development. Technical report, Global Energy Monitor, January 2026.

[65] Cleanview. Bypassing the grid: How data centers are building their own power plants. Technical report, Cleanview, 2026.

[66] Neha Gour, Luis Ortiz, and Edward Maibach. Health implications of the rapid rise of data centers in virginia: an exploratory assessment. *Frontiers in Climate*, 8:1648912, 2026.

Supporting Information for

Air quality and health impacts of Data Center electricity demand in the United States

Yuang Chen[1,2], Shen Wang[3,4], Juan Ramon L Senga[3,5], Andrew Scott White[1,6], Anthony YH Wong[1], Lyssa M Freese[7], Michelle L Bell[8], Noelle E Selin[1,2,9]

[1] Center for Sustainability Science and Strategy, Massachusetts Institute of Technology, Cambridge, MA, United States of America

[2] Institute for Data, Systems and Society, Massachusetts Institute of Technology, Cambridge, MA, United States of America

[3] Center for Energy and Environmental Policy Research, Massachusetts Institute of Technology, Cambridge, MA, United States of America

[4] MIT Energy Initiative, Massachusetts Institute of Technology, Cambridge, MA, United States of America

[5] MIT Climate Policy Center, Massachusetts Institute of Technology, Cambridge, MA, United States of America

[6] Laboratory for Aviation and the Environment, Department of Aeronautics and Astronautics, Massachusetts Institute of Technology, Cambridge, MA, United States of America

[7] Department of Earth System Science, University of California, Irvine, Irvine, CA, United States of America

[8] School of the Environment, Yale University, New Haven, Connecticut, United States of America

[9] Department of Earth, Atmospheric, and Planetary Sciences, Massachusetts Institute of Technology, Cambridge, MA, United States of America

Contents

S1 Supplemental Methods

S1.1 Data center demand mapping

For each Integrated Planning Model (IPM) region, we first determine a region-specific data center electricity share based on the states it intersects, following an approach similar to that used in Knittel et al. [1]. If an IPM region lies entirely within a single state, the regional share is set equal to that state's data center demand share. If an IPM region spans multiple states, the regional share is calculated as the ratio of aggregated state-level data center electricity consumption to aggregated total electricity consumption across those states. This regional share is then applied to the IPM region's total electricity demand to estimate data center electricity demand within that region.

S1.2 US-EGO model update

S1.2.1 Basic model setup

The model has 64 regions, following the region specification in the Integrated Planning Model (IPM) [2]. We acquire hourly electricity demand for all 64 regions in the contiguous United States from the Energy Information Administration (EIA), together with data on interregional electricity transmission capacities and transmission costs. Plant-level generator characteristics, including fuel type, capacity, commissioning year, and geographic location, are compiled from publicly available sources. Plant-level emissions data are used in subsequent post-processing steps to estimate marginal emission impacts.

The optimization step is implemented using the JuMP package in the Julia programming language and solved as a chronological linear economic dispatch problem. The core objective minimizes total system operating cost, including generation costs, transmission costs, and a high penalty on unserved load to ensure feasibility:

$$\underset{x^{\text{gen}},x^{\text{trans}},s}{min}\left(\sum_{i=1}^{N}\sum_{t=1}^{T}x_{it}^{\text{gen}}c_{i}^{\text{gen}}+\sum_{\ell=1}^{L}\sum_{t=1}^{T}x_{\ell t}^{\text{trans}}c_{\ell}^{\text{trans}}+\lambda^{\text{shed}}\sum_{r=1}^{R}\sum_{t=1}^{T}s_{rt}\right), \tag{S1}$$

where x_{it}^{gen} and c_{i}^{gen} represent the generation amount and marginal generation cost of generator i at hour t, and $x_{\ell t}^{\text{trans}}$ and c_{ℓ}^{trans} represent the electricity transfer and associated cost on transmission interface ℓ. The variable s_{rt} denotes load shedding in region r at hour t, penalized at a large constant λ^{shed}. The model is solved over a specified simulation window of hourly periods T.

The US-EGO optimization step includes the following constraints:

1. Generation constraints:

$$x_{it}^{\text{gen}} - x_i^{\text{capacity}} \times \text{profile}_{rt} \leq 0 \qquad \text{if generator } i \text{ is solar or wind in region } r \tag{S2}$$

$$x_{it}^{\text{gen}} - 0.95\, x_i^{\text{capacity}} \leq 0 \qquad \text{if generator } i \text{ is nuclear} \tag{S3}$$

$$x_{it}^{\text{gen}} - x_i^{\text{capacity}} \leq 0 \qquad \text{for other non-hydro generators} \tag{S4}$$

where x_i^{capacity} is the nameplate capacity of generator i, and profile_{rt} is the hourly renewable capacity factor in region r.

Hydropower generators are subject to both instantaneous generation limits and intertemporal reservoir energy constraints that link dispatch decisions across hours. Similarly, grid-scale energy storage resources are represented through intertemporal state-of-charge constraints governing charging and discharging behavior. These formulations are described in detail in the following subsections.

2. Transmission constraints:

$$x_{\ell t}^{\text{trans}} - x_{\ell}^{\text{trans-limit}} \leq 0, \tag{S5}$$

where $x_{\ell}^{\text{trans-limit}}$ is the transfer capacity of transmission interface ℓ. To represent limited interconnection between the Eastern, Western, and ERCOT systems, transfer capacities across these boundaries are set to very small values.

3. Regional power balance:

$$\sum_{i=1}^{N_r} x_{it}^{\text{gen}} + \eta^{\text{trans}} \sum_{\ell \in \mathcal{L}_r^{\text{in}}} x_{\ell t}^{\text{trans}} - \sum_{\ell \in \mathcal{L}_r^{\text{out}}} x_{\ell t}^{\text{trans}} + s_{rt} - L_{rt} = 0, \qquad \forall r \in R,\ t \in T, \tag{S6}$$

where N_r is the number of generators located in region r, L_{rt} is electricity demand in region r at hour t, and η^{trans} represents transmission efficiency losses applied to inflows.

S1.2.2 Generator profile construction

We constructed a harmonized generator-level dataset by integrating multiple authoritative sources to capture the technical, operational, and environmental characteristics of the US power plant fleet. The primary data sources included the National Electric Energy Data System (NEEDS, 2024) for generator attributes, the Emissions & Generation Resource Integrated Database (eGRID, 2023) for plant-level emissions, and the US Energy Information Administration (EIA) Form 923 (2023) for fuel cost data. Additional generator cost information was incorporated from curated datasets from Jenn to address gaps for specific technologies [3].

To ensure consistency across sources, we standardized plant identifiers and focused on active generators. Key generator attributes, such as capacity, heat rate, technology type, and region, were drawn from NEEDS. Emissions data (NO_x, SO_2, and CO_2 output rates, as well as net generation) were merged from eGRID using the harmonized plant ORIS code. We assigned each generator a standardized fuel type based on both reported primary fuel and plant technology.

Data quality is prioritized through systematic cleaning. Outliers in reported emission rates were removed, and for non-emitting or renewable technologies (e.g., wind, solar, hydro, geothermal, nuclear, pumped storage), emission rates are set to near 0. Missing emission factors are imputed using the mean value for each fuel type within a given region, and, if necessary, the national mean for that fuel type. Generators with unresolved missing emissions data are excluded from the final dataset (32 plants, $\leq 0.01\%$ of all capacity). We define peaking units - units typically used to meet peak demand - as natural gas generators operating at annual capacity factors below 25% and oil-fired generators below 10%. 742 natural gas plants and 2164 oil plants are identified as peaker plants.

Fuel cost estimation

Fuel costs for electricity generating units are primarily derived from EIA Form 923, which provides plant-level fuel expenditures and heat input data. Annual fuel costs are constructed by aggregating monthly records and averaging across suppliers to obtain representative plant-level values.

For units with missing or incomplete fuel cost data, we impute `FuelCostTotal` using a regression-based approach applied separately by fuel type (coal, natural gas, and oil). Specifically, we estimate a regularized linear model (ridge regression) using observed units, with fuel cost as the dependent variable and plant characteristics, including heat rate, online year, plant type, and region, as predictors. Categorical variables (plant type and region) are encoded using one-hot encoding, and continuous variables are standardized prior to estimation. The fitted models are then used to predict missing fuel costs.

To ensure physically reasonable values and avoid extreme predictions, imputed fuel costs are bounded within fuel-specific ranges (coal: 5–120 $\$\,\mathrm{MWh}^{-1}$; natural gas: 10–120 $\$\,\mathrm{MWh}^{-1}$; oil: 50–500 $\$\,\mathrm{MWh}^{-1}$) and perturbed with a small multiplicative jitter ($\pm 5\%$) to preserve variability across units.

For non-fossil and special fuel types (e.g., biomass, municipal solid waste, nuclear), missing fuel costs are supplemented using plant-level data from Jenn and Freese et al. [3, 4]. Remaining missing values are filled using mean values by region and fuel type, and subsequently by fuel type alone.

The total fuel cost per unit of electricity generated (`FuelCostTotal`, in $\$\,\mathrm{MWh}^{-1}$) is calculated as:

$$\texttt{FuelCostTotal} = \texttt{FUEL\_COST} \times 10^{-2} \times \texttt{Heat Rate (Btu/kWh)} \times 10^{-3}, \tag{S7}$$

where `FUEL_COST` is reported in cents per MMBtu and `Heat Rate` is generator-specific. This formulation ensures consistency between reported fuel prices and plant-level efficiency.

S1.2.3 Storage modeling

We incorporate grid-scale energy storage units into the model to represent additional operational flexibility in the electricity system. Storage can shift electricity consumption across hours and absorb excess renewable generation, thereby altering dispatch patterns and associated emissions [5]. Storage operational constraints are implemented following a standard linear state-of-charge formulation similar to that used in large-scale power system production-cost models [6]. Each storage unit is characterized by its charging and discharging efficiencies, power capacity (MW), and energy capacity (MWh).

Storage dynamics are represented by intertemporal state-of-charge constraints:

$$s_{bt} = s_{b,t-1} + \eta_b^{\mathrm{c}} q_{bt}^{\mathrm{c}} - \frac{1}{\eta_b^{\mathrm{d}}} q_{bt}^{\mathrm{d}} \qquad \forall b \in B,\ t \in T \tag{S8}$$

$$0 \le s_{bt} \le S_b^{\max} \qquad \forall b \in B,\ t \in T \tag{S9}$$

$$0 \le q_{bt}^{\mathrm{c}} \le P_b^{\max} \qquad \forall b \in B,\ t \in T \tag{S10}$$

$$0 \le q_{bt}^{\mathrm{d}} \le P_b^{\max} \qquad \forall b \in B,\ t \in T \tag{S11}$$

$$s_{b,T} = s_{b,0} \qquad \forall b \in B. \tag{S12}$$

Here, s_{bt} denotes the state of charge (MWh) of storage unit b at hour t, while q_{bt}^{c} and q_{bt}^{d} denote charging and discharging power (MW), respectively. The parameters η_b^{c} and η_b^{d} represent charging and discharging efficiencies. The parameter $S_b^{\max}$ denotes maximum stored energy capacity, and $P_b^{\max}$ denotes maximum charging or discharging power capacity. The cyclic terminal condition prevents artificial depletion of storage at the end of the optimization horizon. Storage operation affects regional electricity balance through net hourly discharge, defined as $q_{bt}^{\mathrm{d}} - q_{bt}^{\mathrm{c}}$. Storage operation does not incur an explicit variable operating cost; instead, charging and discharging decisions are determined endogenously through system-wide cost minimization subject to electricity balance and storage efficiency losses.

S1.2.4 Hydropower reservoir dynamics

Hydropower generators are modeled using a simplified reservoir balance formulation that links hourly generation decisions through intertemporal water availability constraints. Let $g_{i,t}^{\mathrm{hyd}}$ denote hydropower generation for plant i in hour t, and let $E_{i,t}$ denote the corresponding reservoir energy state (MWh equivalent).

Hydropower output is bounded by nameplate capacity:

$$0 \le g_{i,t}^{\mathrm{hyd}} \le \bar{G}_i. \tag{S13}$$

Reservoir dynamics are represented as

$$E_{i,t} = E_{i,t-1} + \bar{G}_i \cdot \phi_{r(i),t} - g_{i,t}^{\text{hyd}} - \psi_{i,t}, \tag{S14}$$

where $\phi_{r(i),t}$ is an exogenous hourly inflow factor derived from regional hydropower availability profiles, and $\psi_{i,t}$ represents spill. Reservoir energy is bounded above by a storage capacity proportional to plant nameplate capacity:

$$0 \leq E_{i,t} \leq H_i \bar{G}_i, \tag{S15}$$

where H_i denotes the assumed number of equivalent storage hours. Initial and terminal reservoir levels are fixed as fractions of total reservoir capacity to avoid end-of-horizon artifacts.

S1.2.5 Linearized unit commitment representation of thermal generators

US-EGO is implemented as a chronological linear economic dispatch model with a linearized unit commitment representation for a subset of large thermal generators. Rather than solving a mixed-integer unit commitment problem with binary commitment, startup, and shutdown variables, we approximate short-run operating inflexibilities using continuous minimum-generation and ramping constraints. This formulation preserves linearity and computational tractability while capturing the primary operational limits governing hourly generator response.

The reduced-form formulation is applied to selected coal and natural-gas combined-cycle (NGCC) units, specifically coal generators with nameplate capacity ≥50 MW and NGCC units with capacity ≥150 MW. Other generators, including gas combustion turbines, oil units, nuclear, renewables, hydro, and smaller thermal units, are modeled using standard dispatch bounds.

Let $g_{i,t}$ denote generation by unit i in hour t (MW), and $\bar{G}_i$ its nameplate capacity. For constrained units, generation is bounded below by a minimum stable output constraint:

$$g_{i,t} \geq \alpha_i \bar{G}_i - \sigma_{i,t}, \qquad \sigma_{i,t} \geq 0, \tag{S16}$$

where α_i is the minimum-load fraction and $\sigma_{i,t}$ is a slack variable penalized in the objective to avoid infeasibility.

Minimum-load parameters are assigned by generator class: $\alpha_i = 0.30$ for coal units and $\alpha_i = 0.40$ for NGCC units. Combustion turbines are not subject to this constraint.

Intertemporal changes in output are represented using ramp variables $r_{i,t}^{+}$ and $r_{i,t}^{-}$:

$$g_{i,t} - g_{i,t-1} = r_{i,t}^{+} - r_{i,t}^{-}, \qquad t \geq 2, \tag{S17}$$

with bounds

$$0 \le r^{+}_{i,t} \le \rho^{+}_{i} \bar{G}_i, \qquad 0 \le r^{-}_{i,t} \le \rho^{-}_{i} \bar{G}_i. \tag{S18}$$

Ramp rates are set to $\rho^{+}_{i} = \rho^{-}_{i} = 0.15$ for coal units and 0.25 for NGCC units.
Initial conditions are approximated using a heuristic starting level:

$$g_{i,1} - g^{*}_{i,0} = r^{+}_{i,1} - r^{-}_{i,1}, \tag{S19}$$

where

$$g^{*}_{i,0} = \begin{cases} \alpha_i \bar{G}_i, & \text{if } \alpha_i > 0, \\ 0, & \text{otherwise.} \end{cases} \tag{S20}$$

This initialization provides a plausible operating point without reconstructing pre-horizon commitment status.
To limit excessive cycling in the continuous formulation, ramping and minimum-generation slack are penalized in the objective:

$$\sum_{i \in \mathcal{G}^{\mathrm{RF}}} \sum_{t} c^{\mathrm{ramp}}_{i} \left(r^{+}_{i,t} + r^{-}_{i,t} \right) \; + \; \lambda^{\mathrm{pmin}} \sum_{i \in \mathcal{G}^{\mathrm{RF}}} \sum_{t} \sigma_{i,t}, \tag{S21}$$

where $\mathcal{G}^{\mathrm{RF}}$ is the set of constrained generators. We set $c^{\mathrm{ramp}}_{i} = 1.0$ for coal units and 0.7 for NGCC units, and $\lambda^{\mathrm{pmin}} = 100$.

S1.2.6 Model output validation

We evaluate the performance of the US-EGO dispatch model by comparing simulated generation against reported data for 2023 (Figure S1). At the regional level (panel a), total electricity generation by fuel type is compared across major US electricity markets, with model estimates in close agreement with values reported by the US Energy Information Administration (EIA) across coal, natural gas, nuclear, and renewable generation. At the plant level (panel b), simulated annual generation for individual units is compared against eGRID-reported values, showing strong agreement across a wide range of plant sizes and fuel types, with most observations clustered near the 1:1 line. Deviations for some solar units reflect limitations in available commissioning data: while plant capacity is known, precise online dates within 2023 are not always available, leading to some units being represented as operating for the full year in the model. This results in a systematic upward bias for a subset of solar plants but does not affect the aggregate representation of renewable generation or system-level dispatch patterns. Overall, the model captures both regional generation mixes and unit-level production with sufficient accuracy to support attribution of marginal generation and emissions responses.

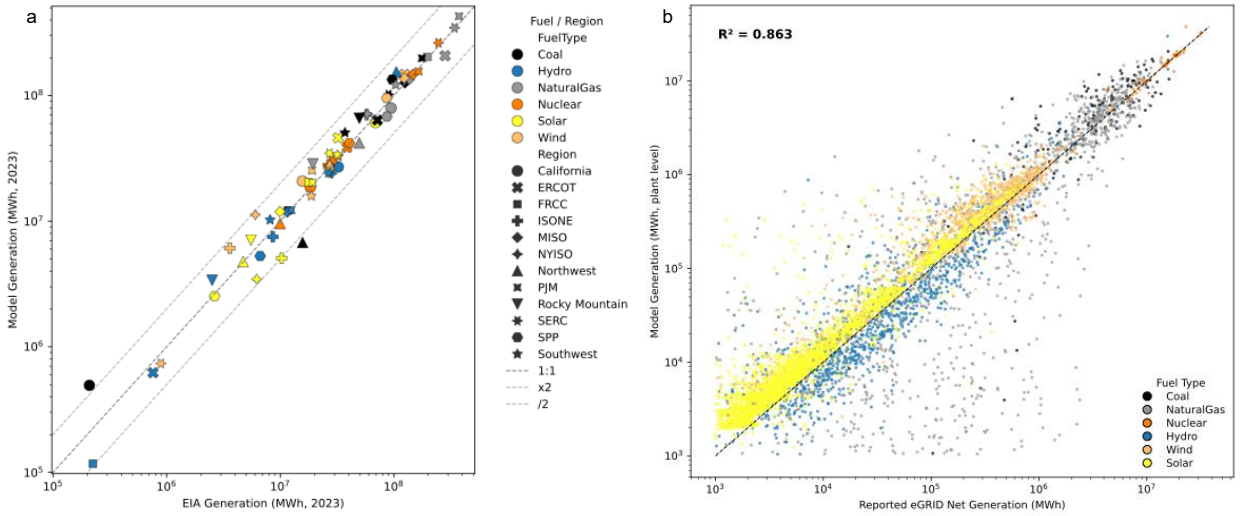

Figure S1: Validation of US-EGO electricity generation in 2023. (a) Regional electricity generation by fuel type from US-EGO compared with reported values from the US Energy Information Administration (EIA) across major electricity markets. (b) Plant-level comparison of simulated annual generation from US-EGO and reported generation from the eGRID database for individual generating units. Each point represents a plant, and the dashed line indicates the 1:1 relationship.

S1.3 GEOS-Chem High Performance model validation

We evaluate the performance of the GCHP baseline simulation against ground-based observations from the US EPA Air Quality System (AQS) (Figures S2, S3). Spatial patterns of annual mean $PM_{2.5}$ and MDA8-O_3 are well reproduced, with higher concentrations across the eastern United States and lower levels in the western regions (Figure S2 a,c). At monitoring sites, the model captures broad spatial gradients but exhibits a positive bias for both pollutants, particularly for $PM_{2.5}$ in the eastern United States (Figure S2b). Regression analysis shows moderate agreement for $PM_{2.5}$ (N = 933, R = 0.41, RMSE = 3.56 μg m^{-3}) and stronger agreement for O_3 (N = 1292, R = 0.65, RMSE = 7.5 ppb), with mean biases of 1.15 μg m^{-3} and 6.3 ppb, respectively (Figure S3). These biases are consistent with previously documented GEOS-Chem behavior, including overestimation of nitrate aerosol under ammonia-rich conditions and known evaluation differences in MDA8-O_3 metrics [7, 8]. Importantly, as our analysis focuses on concentration differences ($\Delta PM_{2.5}$ and ΔO_3) resulting from emissions perturbations, the spatial patterns of attributable impacts are only weakly influenced by baseline model bias.

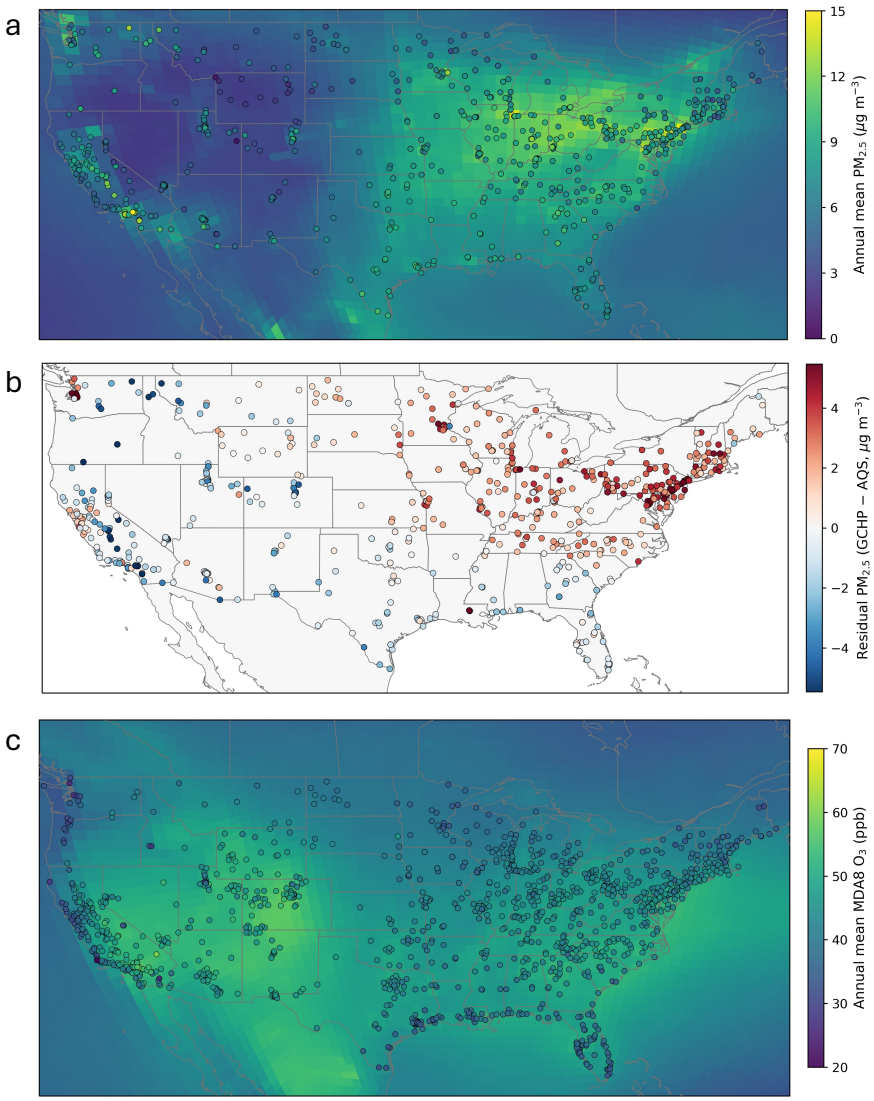

Figure S2: Evaluation of GCHP baseline simulation against AQS observations in 2023. (a) Annual mean $PM_{2.5}$ concentrations from GCHP (color shading) with AQS monitoring station observations overlaid (circles). (b) Spatial distribution of $PM_{2.5}$ residuals (GCHP - AQS) at monitoring locations. (c) Annual mean MDA8-O_3 concentrations from GCHP with AQS observations overlaid. Model simulations use full-chemistry GCHP driven by NEI emissions within the United States and CEDS emissions elsewhere.

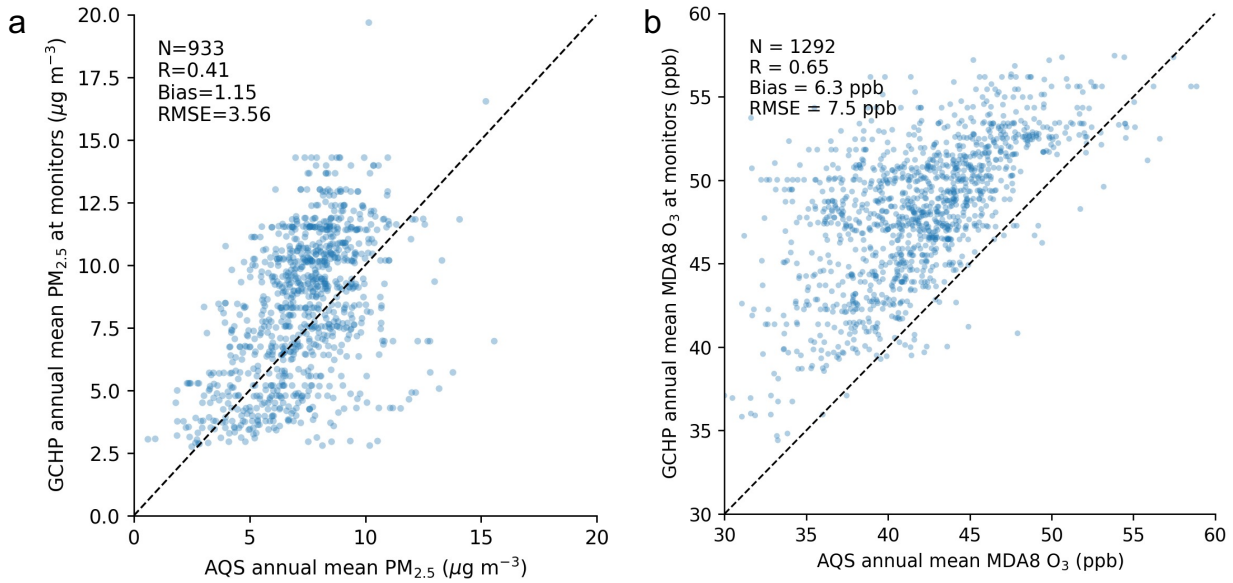

Figure S3: Statistical comparison between GCHP simulations and AQS observations. (a) Comparison of annual mean $PM_{2.5}$ concentrations at monitoring sites (N = 933). (b) Comparison of annual mean MDA8-O_3 concentrations (N = 1292). Each point represents a monitoring site, and the dashed line indicates the 1:1 relationship. Reported statistics include Pearson correlation coefficient (R), mean bias (model - observation), and root-mean-square error (RMSE).

S1.4 Health impact calculation

We estimate premature mortality associated with changes in ground-level $PM_{2.5}$ and O_3 concentrations by applying established concentration-response functions (CRFs) to gridded population and baseline mortality data. We use the Gridded Population of the World v4.11 dataset at 30 arc-second resolution [9]. Age-specific baseline mortality rates are obtained from the World Health Organization (WHO) [10]. Since the air quality modeling grid is coarser than the population grid, pollutant concentrations are spatially matched by assigning each population cell the pollutant level from the overlying coarser grid cell. Premature mortality for each grid cell and age group is calculated using the following equation:

$$\Delta M_i = M_0 \frac{RR_i - RR_0}{RR_0} \tag{S22}$$

where ΔM_i is the change in mortality under scenario i (with organization's impact), M_0 is the baseline number of mortalities (without organization's impact), RR_i is the relative risk from pollutant exposure in scenario i, and RR_0 is the baseline risk.

For $PM_{2.5}$, we apply the CRF from the Global Exposure Mortality Model (GEMM) for non-communicable diseases and lower respiratory infections [11]. For O_3, we estimate mortality due to both all-cause and respiratory diseases using the log-linear CRF based on annual mean MDA8-O_3 from Turner et al. [12], with relative risk estimates of 1.02 (95% CI: 1.01–1.04) and 1.12 (95% CI: 1.08–1.16), respectively.

S2 Supplemental Results

S2.1 $PM_{2.5}$ concentration in Iowa and Nebraska

Figure S4 shows the spatial distribution of Δ surface nitrate (NO_3^-) and ammonium (NH_4^+) concentrations attributable to data center electricity demand from GCHP simulations. Both species exhibit elevated and co-located responses across the Midwest and Ohio Valley, with closely aligned spatial patterns. This co-occurrence is consistent with enhanced formation of ammonium nitrate (NH_4NO_3) under ammonia-rich conditions. The similar spatial extent and magnitude of ΔNO_3^- and ΔNH_4^+ further support nitrate as the dominant contributor to the $PM_{2.5}$ response.

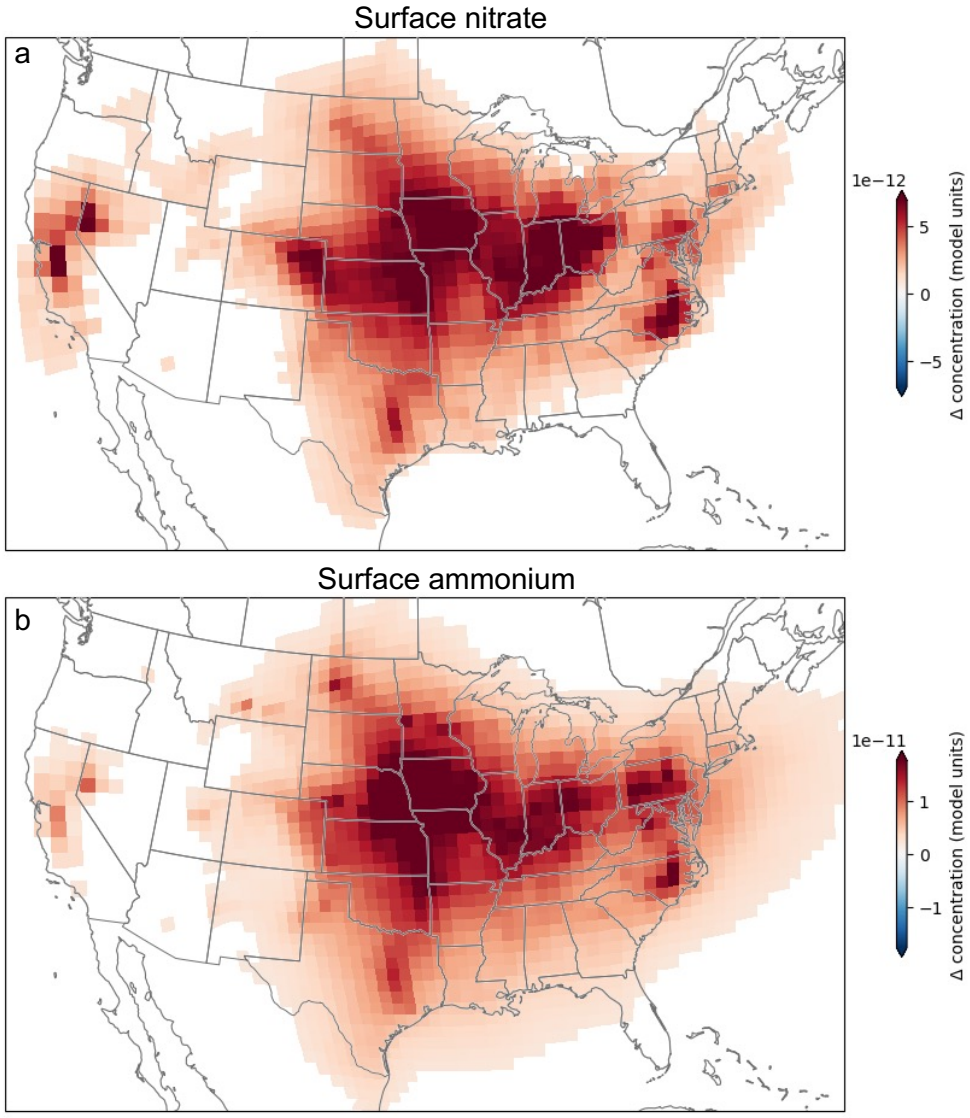

Figure S4: Changes in annual mean surface nitrate (NO_3^-; a) and ammonium (NH_4^+; b) concentrations attributable to data center electricity demand, simulated using GEOS-Chem High Performance.

Figure S5 shows that elevated $\Delta PM_{2.5}$ concentrations in Iowa and Nebraska are spatially aligned with the locations of coal-fired power plants. The highest concentration responses occur in proximity to a small number of large generating units.

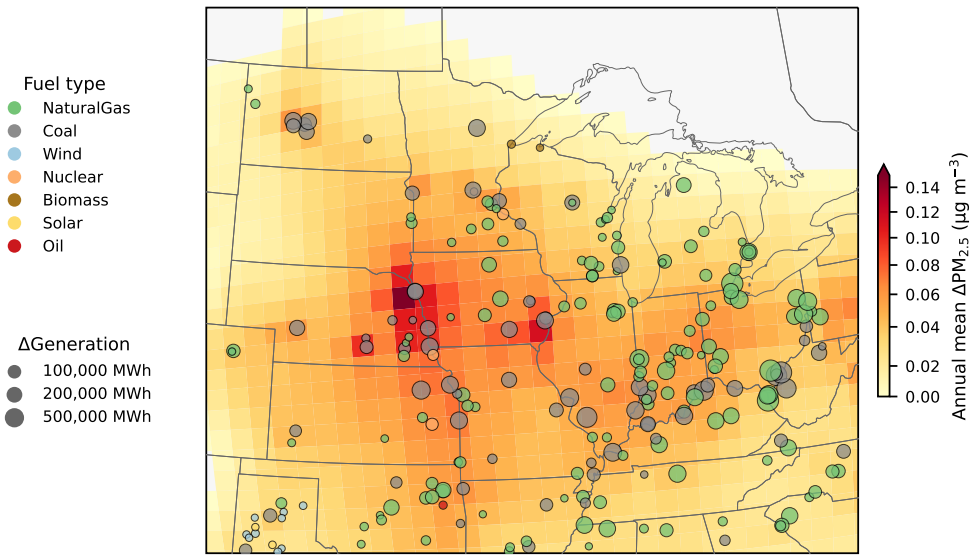

Figure S5: Spatial relationship between $\Delta PM_{2.5}$ and coal-fired power plants in the central United States. Color shading shows annual mean $\Delta PM_{2.5}$ attributable to data center electricity demand, and circles indicate locations and generation of electricity generating units attributable to data center load.

S2.2 MDA8-O_3 seasonal patterns

Figure S6 shows the seasonal response of MDA8 O_3 attributable to data center electricity demand from GCHP simulations. In summer (June, July, August), ΔMDA8 O_3 is broadly positive across most of the United States, with the largest enhancements occurring in the eastern US and extending downwind of major emission regions, reflecting active photochemistry and NO_x-limited ozone production. In contrast, wintertime (December, January, February) responses are generally negative and more spatially localized, particularly near major generation regions, consistent with ozone titration under high-NO_x and low-photochemical conditions.

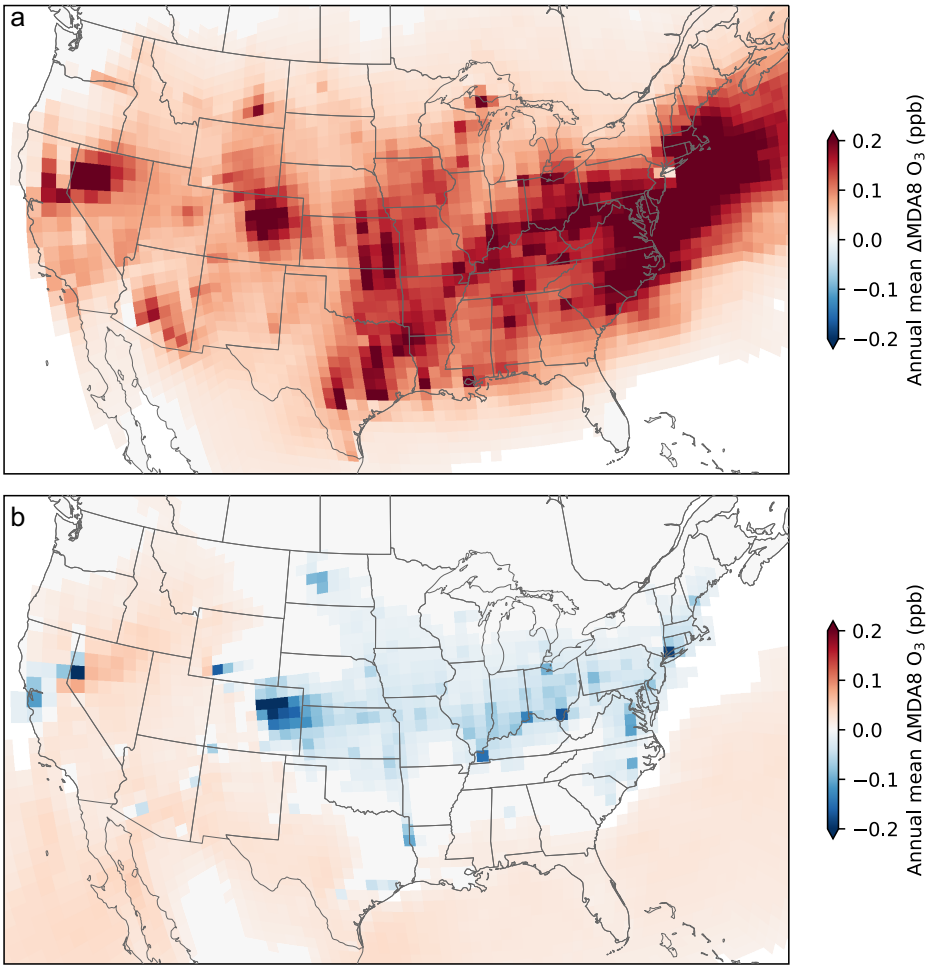

Figure S6: Seasonal MDA8-O_3 response attributable to data center electricity demand. (a) Summer (June, July, August) and (b) winter (December, January, February) ΔMDA8-O_3 concentrations.

S2.3 State level mortality results

Table S1: State-level data center-attributable, EGU-attributable, and baseline mortality estimates. Uncertainty ranges represent 95% confidence intervals.

State	DC load (TWh yr^{-1})	DC-attributable mortality	EGU-attributable mortality	Baseline mortality	DC contribution to EGU mortality (%)	DC contribution to baseline mortality (%)
Texas	21.8	69 (59–79)	1284 (1105–1463)	241773 (241497–242048)	5.36	0.028
Pennsylvania	4.6	36 (32–41)	610 (539–680)	111969 (111846–112091)	5.98	0.033
Ohio	2.4	36 (31–40)	626 (552–701)	100912 (100784–101038)	5.70	0.035
Illinois	7.5	35 (31–39)	623 (546–700)	114876 (114738–115012)	5.62	0.030
North Carolina	2.7	29 (25–34)	656 (564–747)	90667 (90525–90807)	4.47	0.032
Virginia	33.9	25 (21–29)	430 (372–488)	74444 (74352–74534)	5.90	0.034
New York	4.1	24 (21–26)	427 (364–490)	145342 (145241–145443)	5.53	0.016
Missouri	1.0	23 (21–26)	527 (468–586)	53941 (53835–54045)	4.41	0.043
Indiana	0.2	22 (20–25)	414 (366–461)	58554 (58469–58637)	5.42	0.038
California	9.3	22 (18–26)	440 (378–503)	216994 (216890–217096)	5.04	0.010
Michigan	0.5	21 (19–23)	372 (331–413)	85984 (85910–86057)	5.66	0.024
Georgia	6.2	19 (16–22)	476 (408–545)	92170 (92067–92273)	4.05	0.021
Maryland	0.1	18 (15–21)	288 (252–324)	53528 (53469–53588)	6.31	0.034
New Jersey	4.0	18 (16–20)	248 (194–302)	92682 (92599–92764)	7.13	0.019
Minnesota	0.8	17 (15–18)	258 (233–282)	47419 (47370–47467)	6.53	0.035
Tennessee	1.3	16 (14–19)	358 (311–404)	57422 (57347–57497)	4.60	0.029
Iowa	6.2	15 (13–16)	245 (221–269)	26857 (26810–26904)	6.01	0.055
Kentucky	1.6	14 (13–16)	299 (261–336)	38795 (38733–38857)	4.83	0.037
Wisconsin	0.1	14 (12–15)	246 (221–271)	50836 (50788–50883)	5.66	0.027
Oklahoma	1.2	14 (12–15)	238 (209–267)	34376 (34327–34424)	5.72	0.040
Florida	1.4	13 (11–15)	514 (414–614)	176646 (176520–176773)	2.59	0.008
Kansas	0.0	13 (12–15)	229 (203–254)	25726 (25681–25772)	5.81	0.052
Nebraska	4.0	12 (11–13)	242 (219–265)	16537 (16491–16583)	5.02	0.074
Massachusetts	1.1	12 (10–14)	170 (141–199)	57268 (57228–57307)	6.94	0.021
Alabama	1.5	10 (9–12)	216 (183–249)	43334 (43286–43382)	4.74	0.024
South Carolina	2.0	10 (9–12)	234 (199–270)	43467 (43415–43519)	4.31	0.023
Arizona	6.3	10 (8–12)	106 (82–130)	62059 (62031–62086)	9.43	0.016
Arkansas	0.0	10 (8–11)	226 (196–255)	26662 (26615–26709)	4.26	0.036
Louisiana	0.1	9 (7–10)	208 (172–243)	40075 (40027–40124)	4.11	0.021
Colorado	1.5	8 (5–11)	201 (177–225)	47545 (47504–47586)	4.14	0.018

State	DC load (TWh yr^{-1})	DC-attributable mortality	EGU-attributable mortality	Baseline mortality	DC contribution to EGU mortality (%)	DC contribution to baseline mortality (%)
Connecticut	0.3	8 (6–10)	136 (112–159)	31941 (31909–31972)	5.89	0.025
Mississippi	0.0	6 (5–7)	145 (124–166)	27257 (27225–27289)	4.41	0.023
West Virginia	0.0	6 (5–7)	106 (93–120)	16421 (16399–16443)	5.36	0.035
Nevada	3.4	5 (5–6)	31 (25–37)	27341 (27334–27349)	17.56	0.020
Utah	2.6	4 (3–5)	47 (41–54)	26764 (26754–26774)	8.46	0.015
New Mexico	0.4	4 (3–4)	57 (49–65)	19439 (19427–19451)	6.81	0.020
South Dakota	0.1	4 (3–4)	57 (52–63)	7466 (7455–7477)	6.18	0.047
Delaware	0.0	2 (2–3)	41 (36–47)	8191 (8182–8199)	5.91	0.030
Rhode Island	0.0	2 (2–3)	33 (27–39)	9150 (9142–9158)	7.30	0.026
Idaho	0.1	2 (2–2)	16 (14–18)	14338 (14335–14341)	12.04	0.013
New Hampshire	0.0	2 (1–2)	27 (23–31)	11443 (11437–11449)	6.45	0.015
D.C.	0.0	2 (1–2)	26 (23–29)	5050 (5045–5055)	6.37	0.033
North Dakota	3.9	2 (1–2)	29 (27–32)	4999 (4993–5005)	5.33	0.031
Montana	0.6	1 (1–2)	18 (16–20)	7313 (7309–7316)	8.22	0.020
Wyoming	1.9	1 (1–2)	29 (25–32)	5268 (5262–5274)	5.17	0.028
Washington	5.2	1 (1–1)	13 (11–14)	9838 (9836–9841)	6.87	0.009
Vermont	0.0	1 (1–1)	11 (10–13)	5634 (5631–5636)	6.88	0.014
Maine	0.0	1 (1–1)	13 (11–15)	5867 (5865–5870)	5.84	0.013
Oregon	6.4	0 (0–0)	2 (1–2)	1567 (1566–1567)	11.38	0.011

S2.4 Spatial distribution of mortality risks relative to data center locations

Figures S7–S9 provide additional details on the spatial relationship between data center locations and attributable mortality. Figure S7 classifies counties within each electricity market as hosting, neighboring, or farther from hyperscale facilities and compares mortality rate distributions across these categories. Figures S8 and S9 examine the relationship between mortality rates and distance to the nearest large-scale data center at the national and market levels, respectively. Major electricity markets correspond approximately to the following regions: ISO-NE (New England), NYISO (New York), PJM (Mid-Atlantic), MISO (Midwest), SPP (central US), ERCOT (Texas), CAISO (California), Southeast (non-ISO southeastern states), and WECC (western US outside CAISO).

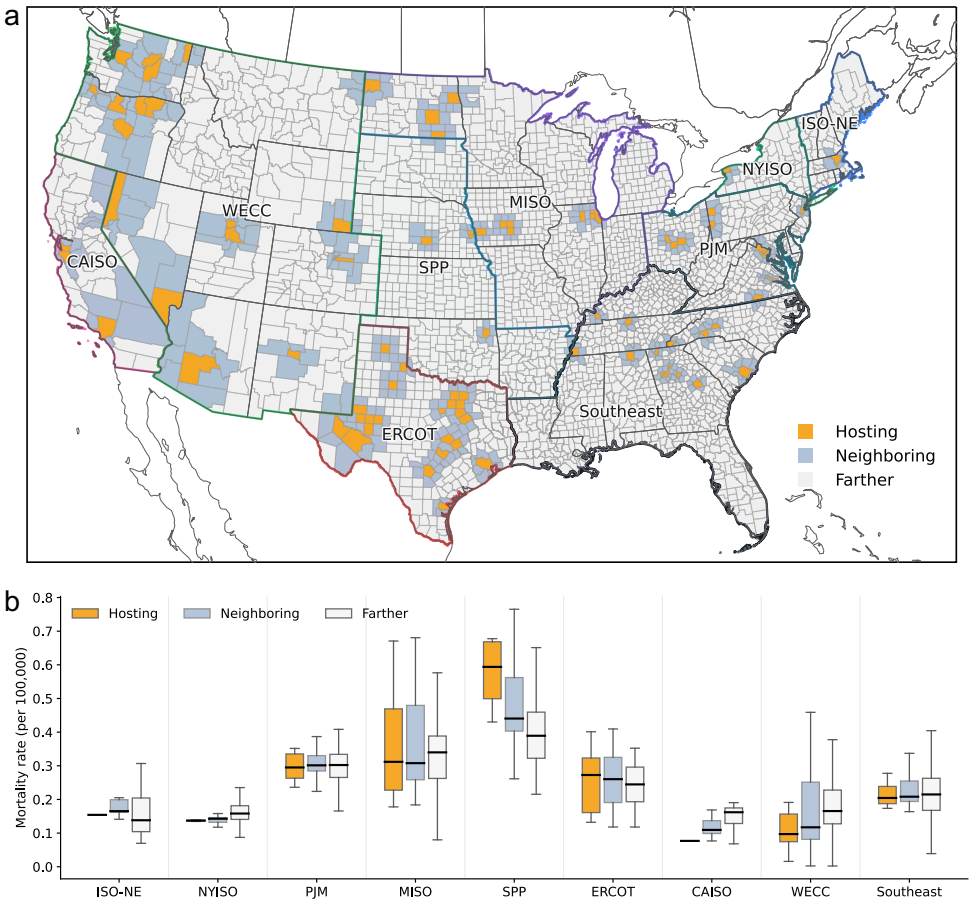

Figure S7: County classification and mortality rates by proximity to hyperscale data centers. (a) Counties classified as hosting, neighboring, or farther from hyperscale data center facilities within each electricity market. (b) Distribution of attributable mortality rates (deaths per million) across county classes by market. Boxes show interquartile ranges with medians; whiskers denote variability within each category.

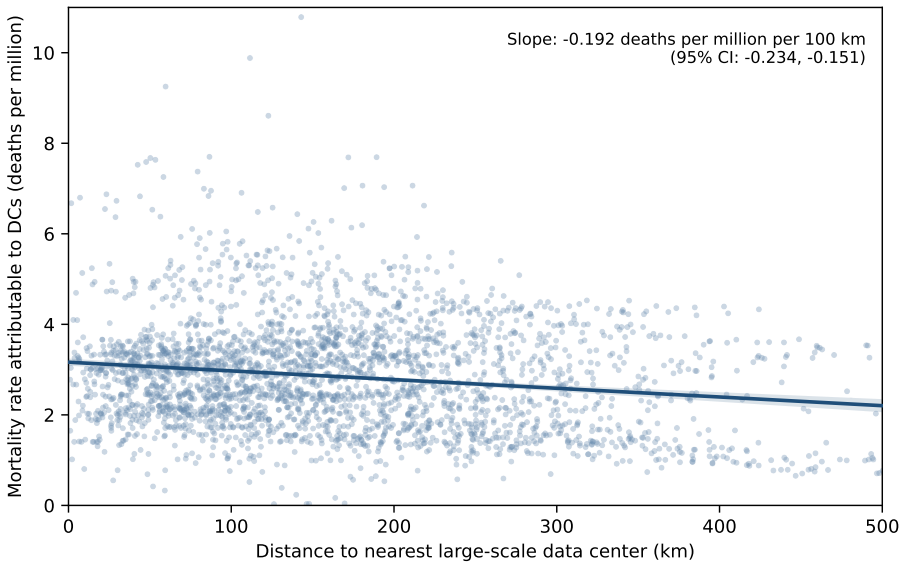

Figure S8: County-level attributable mortality rates versus distance to the nearest large-scale data center. The solid line shows the fitted linear relationship, indicating a weak negative gradient; shading denotes the 95% confidence interval.

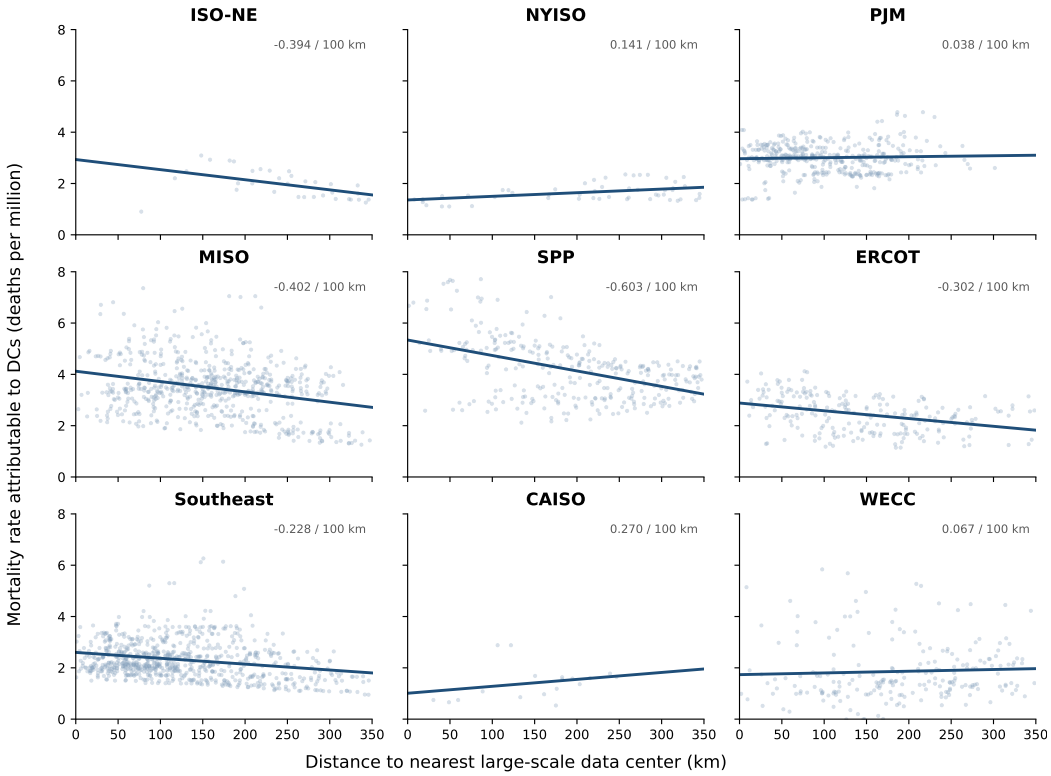

Figure S9: County-level mortality rates plotted against distance to the nearest large-scale data center for each electricity market. Lines show fitted linear relationships, illustrating heterogeneous but generally small distance gradients across regions.

S2.5 Spatial drivers of AIAN mortality-rate outliers

Figure 4b shows that most within-state racial and ethnic differences in attributable mortality rates are centered near zero. However, several states exhibit elevated relative mortality rates for American Indian and Alaska Native (AIAN) populations, most notably Nevada, Colorado, Montana, Utah, and Nebraska. To better understand these outliers, Figure S10 compares the spatial distribution of attributable mortality rates with the distribution of AIAN populations within each state.

The elevated AIAN mortality rates in these states are primarily associated with the geographic overlap between AIAN population centers and regions experiencing above-average attributable mortality rates. In Nevada, for example, 61% of the AIAN population resides in grid cells with mortality rates above the state average, compared with 23% of the total state population. Similar patterns are observed in Colorado, Montana, and Utah. These results suggest that the largest within-state disparities are driven by the spatial concentration of subgroup populations within higher-impact regions rather than by uniformly elevated mortality burdens across entire states. Nebraska represents a contrasting case, where AIAN populations exhibit only modest differences in exposure relative to the state population despite an elevated relative mortality rate.

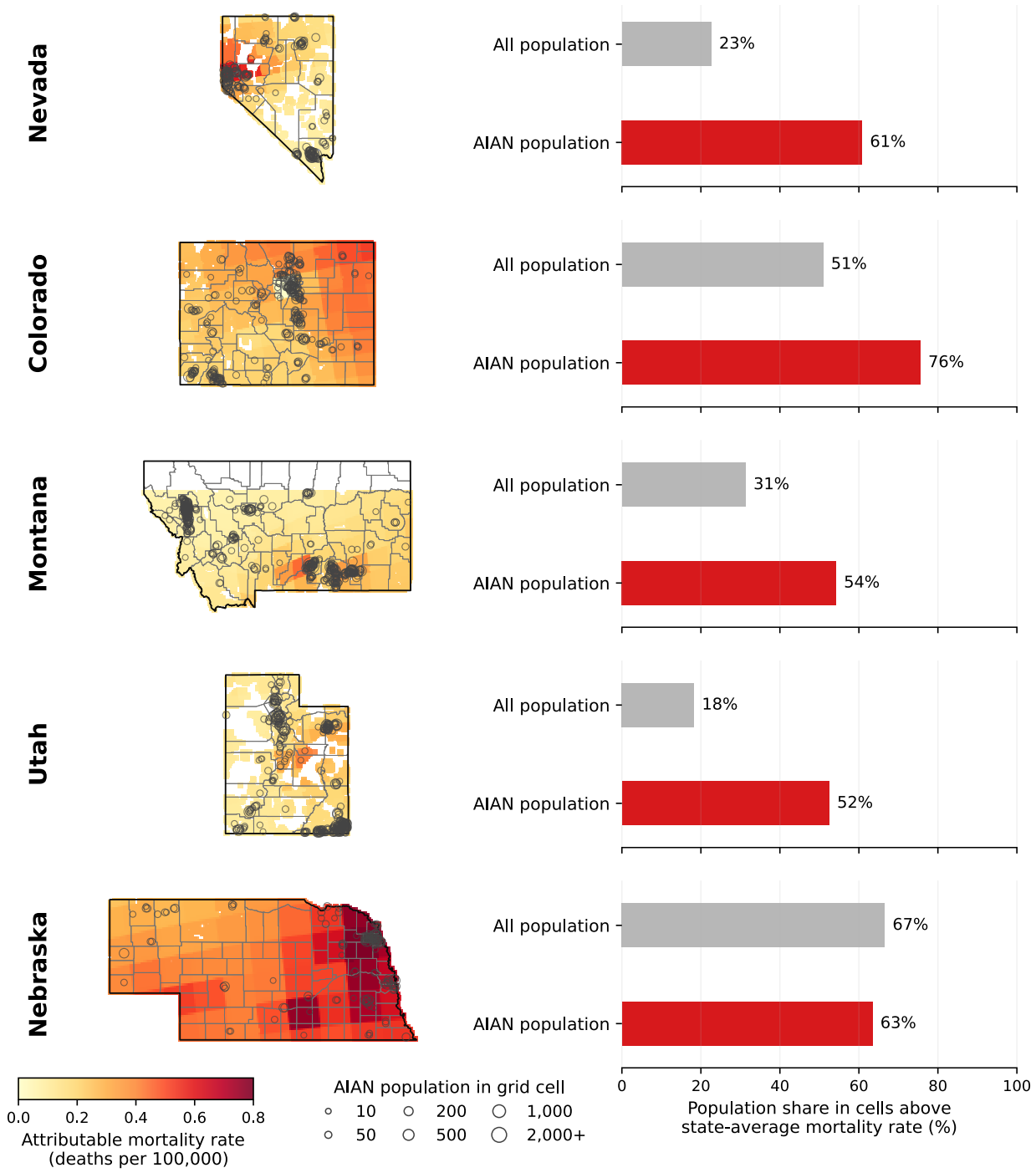

Figure S10: Diagnostic analysis of states with the largest positive AIAN relative mortality rates in Figure 4b. Maps show attributable mortality rates from data center electricity demand (deaths per 100,000 population) overlaid with AIAN population represented by open circles scaled to population size. Bar plots compare the fraction of the total state population and AIAN population located in grid cells with attributable mortality rates above the state average. Elevated AIAN mortality rates generally occur where AIAN populations are disproportionately concentrated within higher-impact regions of a state rather than in states with the highest overall attributable mortality burdens.

S2.6 Comparisons between GCHP- and ISRM-based estimates

Figures S11 and S12 provide additional context for interpreting the $PM_{2.5}$ response across modeling frameworks and chemical regimes. Figure S11 compares annual mean $PM_{2.5}$ concentrations attributable to data center electricity demand estimated using the reduced-form InMAP ISRM and the full-chemistry GCHP model, showing broadly consistent large-scale spatial patterns with differences in magnitude and spatial detail reflecting model structure and treatment of atmospheric chemistry.

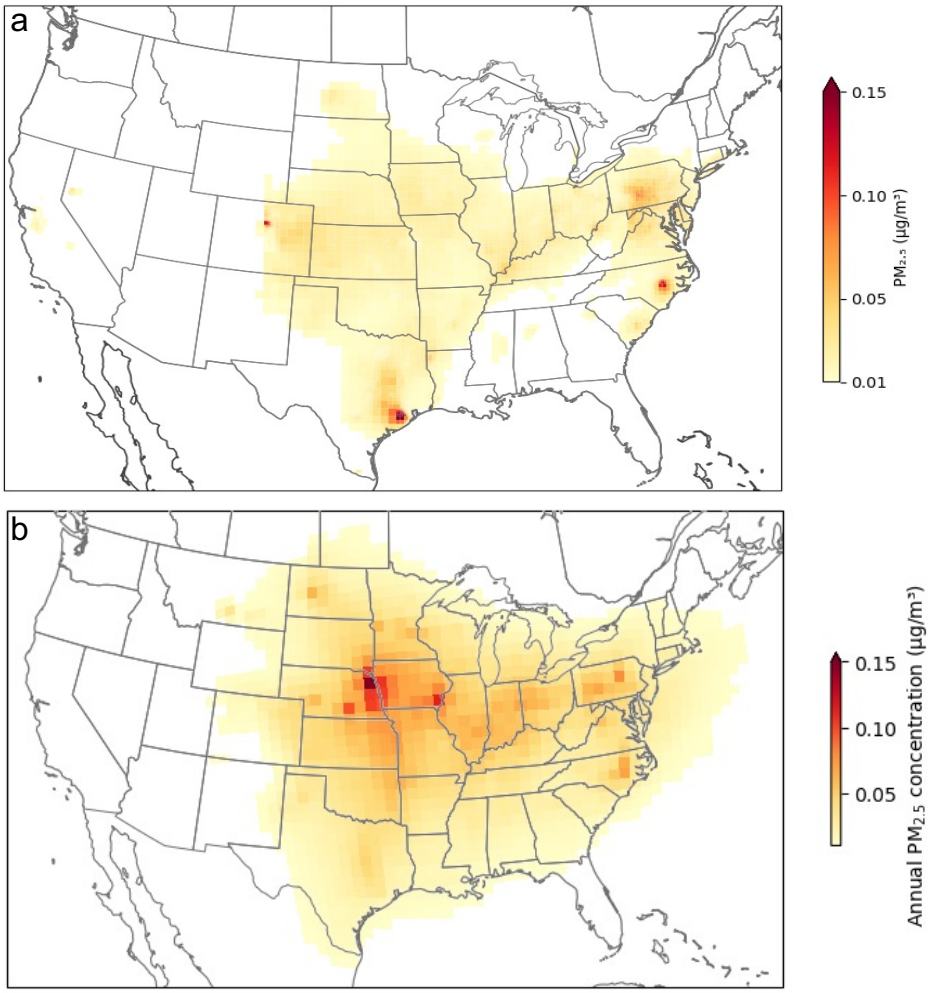

Figure S11: Annual mean $PM_{2.5}$ concentrations attributable to data center electricity demand estimated using (a) the InMAP ISRM and (b) the GCHP chemical transport model.

To further interpret these differences, Figure S12 characterizes changes in ammonia availability using a measure of NH_3 richness defined as $R = NH_3/(NO_x + 2SO_2)$ in molar equivalents. We compute the change in this ratio between 2008 and 2019 as $\log_2(R_{2019}/R_{2008})$ using CEDS gridded emissions, where positive values indicate increasing NH_3 abundance relative to acidic precursors. As shown in Figure S13, most regions of the United States exhibit positive changes in NH_3 richness, reflecting substantial declines in NO_x and SO_2 emissions over this period. This shift toward more ammonia-rich conditions increases the

sensitivity of secondary inorganic aerosol formation to incremental NO_x and SO_2 emissions, providing context for the stronger and more spatially extensive $PM_{2.5}$ responses simulated by GCHP relative to reduced-form approaches.

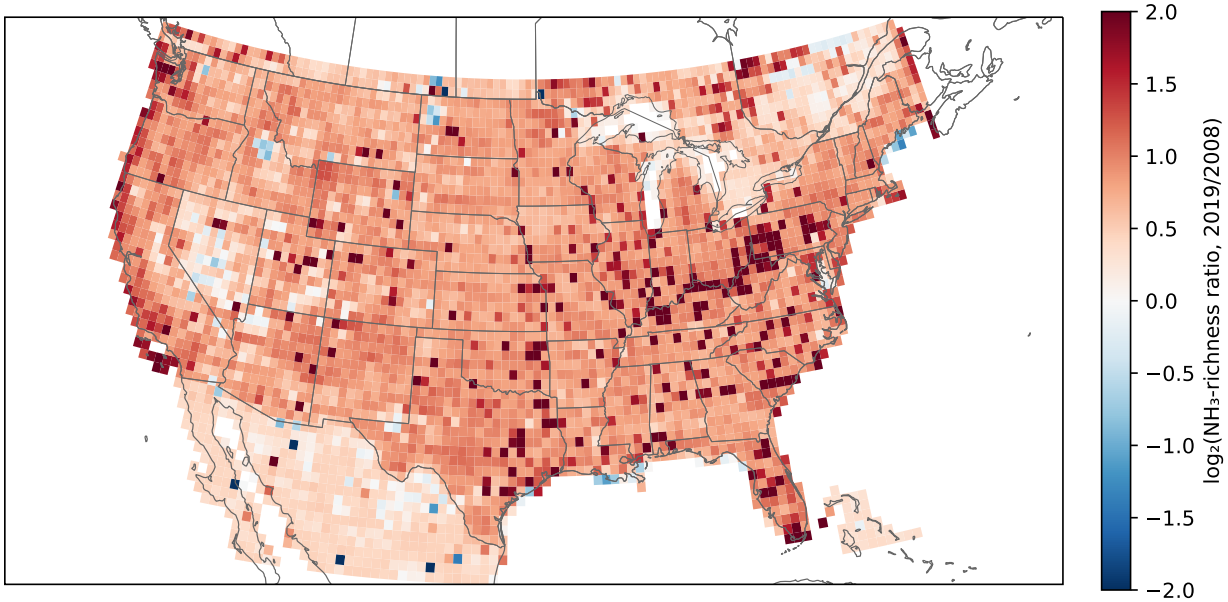

Figure S12: Spatial distribution of the change in NH_3 richness between 2008 and 2019, defined as $\log_2(R_{2019}/R_{2008})$, where $R = NH_3/(NO_x + 2SO_2)$ in molar equivalents.

SI References

[1] Christopher R Knittel, Juan Ramon L Senga, and Shen Wang. Flexible data centers and the grid: Lower costs, higher emissions? Technical report, National Bureau of Economic Research, 2025. NBER Working Paper.

[2] US Environmental Protection Agency. Epa's power sector modeling platform v6 using ipm summer 2021 reference case. https://www.epa.gov/power-sector-modeling/epas-power-sector-modeling-platform-v6-using-ipm-summer-2021-reference-case, 2021. Accessed: March 31, 2025.

[3] A. Jenn. The future of electric vehicle emissions in the united states. Presented at the Transportation Research Board 97th Annual Meeting, Washington, DC, 2018. Paper No. 18-03325.

[4] L. M. Freese, G. P. Chossière, S. D. Eastham, A. Jenn, and N. E. Selin. Nuclear power generation phase-outs redistribute us air quality and climate-related mortality risk. *Nat. Energy*, 8(5):492–503, 2023.

[5] Peter D Lund, Juuso Lindgren, Jani Mikkola, and Jyri Salpakari. Review of energy system flexibility measures to enable high levels of variable renewable electricity. *Renewable and sustainable energy reviews*, 45:785–807, 2015.

[6] MIT Energy Initiative and Princeton University ZERO Lab. GenX: a configurable power system capacity expansion model for studying low-carbon energy futures. https://github.com/GenXProject/GenX, 2023. Accessed: 2025-05-30.

[7] JM Walker, S Philip, RV Martin, and JH Seinfeld. Simulation of nitrate, sulfate, and ammonium aerosols over the united states. *Atmos. Chem. Phys.*, 12(22):11213–11227, 2012.

[8] Katherine R. Travis and Daniel J. Jacob. Systematic bias in evaluating chemical transport models with maximum daily 8 h average (mda8) surface ozone for air quality applications: A case study with geos-chem v9.02. *Geosci. Model Dev.*, 12(8):3641–3648, 2019.

[9] Center for International Earth Science Information Network. Gridded population of the world, version 4 (gpwv4): National identifier grid, revision 11. https://405sedac.ciesin.columbia.edu/data/set/gpw-v4-national-identifier-grid-406rev11, 2017.

[10] World Health Organization. Who methods and data sources for country-level causes of death 2000–2016. https://terrance.who.int/mediacentre/data/ghe/541healthinfo/Deaths/GHE2016_COD_methods.pdf, 2018.

[11] R. Burnett, H. Chen, M. Szyszkowicz, N. Fann, B. Hubbell, III Pope, C. A., J. S. Apte, M. Brauer, A. Cohen, S. Weichenthal, J. Coggins, Q. Di, B. Brunekreef, J. Frostad, S. S. Lim, H. Kan, K. D. Walker, G. D. Thurston, R. B. Hayes, C. C. Lim, M. C. Turner, M. Jerrett, D. Krewski, S. M. Gapstur, W. R. Diver, B. Ostro, D. Goldberg, D. L. Crouse, R. V. Martin, P. Peters, L. Pinault, M. Tjepkema, A. van Donkelaar, P. J. Villeneuve, A. B. Miller, P. Yin, M. Zhou, L. Wang, N. A. H. Janssen, M. Marra, R. W. Atkinson, H. Tsang, T. Q. Thach, J. B. Cannon, R. T. Allen, J. E. Hart, F. Laden, G. Cesaroni, F. Forastiere, G. Weinmayr, A. Jaensch, G. Nagel, H. Concin, and J. V. Spadaro. Global estimates of mortality associated with long-term exposure to outdoor fine particulate matter. *Proc. Natl. Acad. Sci. U.S.A.*, 115(38):9592–9597, 2018.

[12] M. C. Turner, M. Jerrett, III Pope, C. A., D. Krewski, S. M. Gapstur, W. R. Diver, B. S. Beckerman, J. D. Marshall, J. Su, D. L. Crouse, et al. Long-term ozone exposure and mortality in a large prospective study. *Am. J. Respir. Crit. Care Med.*, 193(10):1134–1142, 2016.